applied sciences

MDPI

Article

Geophysical and Geochemical Exploration of the Pockmark Field in the Gulf of Patras: New Insights on Formation, Growth and Activity

Dimitris Christodoulou [1], George Papatheodorou [1,*], Maria Geraga [1], Giuseppe Etiope [2], Nikos Giannopoulos [1], Sotiris Kokkalas [3], Xenophon Dimas [1], Elias Fakiris [1], Spyros Sergiou [1], Nikos Georgiou [1], Efthimios Sokos [4] and George Ferentinos [1]

[1] Laboratory of Marine Geology and Physical Oceanography (Oceanus Lab), Department of Geology, University of Patras, Rio, 26500 Patras, Greece; dchristo@upatras.gr (D.C.); mgeraga@upatras.gr (M.G.); up1052511@upnet.gr (N.G.); xendimas@upatras.gr (X.D.); fakiris@upatras.gr (E.F.); sergiou@upatras.gr (S.S.); nikos.georgiou@unive.it (N.G.); gferen@upatras.gr (G.F.)
[2] Istituto Nazionale di Geofisica e Vulcanologia, Sezione Roma 2, 00143 Rome, Italy; giuseppe.etiope@ingv.it
[3] Laboratory of Structural Geology & Tectonics, Department of Geology, University of Patras, 26504 Patras, Greece; skokalas@upatras.gr
[4] Seismological Laboratory, Department of Geology, University of Patras, 26500 Patras, Greece; esokos@upatras.gr
* Correspondence: gpapathe@upatras.gr

Abstract: The Patras Gulf Pockmark field is located in shallow waters offshore Patras City (Greece) and is considered one of the most spectacular and best-documented fluid seepage activities in the Ionian Sea. The field has been under investigation since 1996, though surveying was partially sparse and fragmentary. This paper provides a complete mapping of the field and generates new knowledge regarding the fluid escape structures, the fluid pathways, their origin and the link with seismic activity. For this, data sets were acquired utilising high-resolution marine remote sensing techniques, including multibeam echosounders, side-scan sonars, sub-bottom profilers and remotely operated vehicles, and laboratory techniques focusing on the chemical composition of the escaping fluids. The examined morphometric parameters and spatial distribution patterns of the pockmarks are directly linked to tectonic structures. Acoustic anomalies related to the presence of gas in sediments and in the water column document the activity of the field at present and in the past. Methane is the main component of the fluids and is of microbial origin. Regional and local tectonism, together with the Holocene sedimentary deposits, appear to be the main contributors to the growth of the field. The field preserves evidence that earthquake activity prompts the activation of the field.

Keywords: pockmarks; gas in marine sediments; gas seepage; earthquake; faults; microbial gas; Patras Gulf

Citation: Christodoulou, D.; Papatheodorou, G.; Geraga, M.; Etiope, G.; Giannopoulos, N.; Kokkalas, S.; Dimas, X.; Fakiris, E.; Sergiou, S.; Georgiou, N.; et al. Geophysical and Geochemical Exploration of the Pockmark Field in the Gulf of Patras: New Insights on Formation, Growth and Activity. *Appl. Sci.* **2023**, *13*, 10449. https://doi.org/10.3390/app131810449

Academic Editor: Marta Pérez Arlucea

Received: 7 August 2023
Revised: 2 September 2023
Accepted: 12 September 2023
Published: 19 September 2023

1. Introduction

Pockmarks are depressions in the seabed that form due to the focused expulsion of fluids from subsurface sedimentary layers through the seafloor [1]. Fluids can be aqueous liquids, like porewater [2–5] and/or seeping hydrocarbons, especially methane, which can be of microbial origin [6], thermogenic origin [7–9] or a mixture of them [10–13]. Pockmarks associated with the venting of gas fluids have become widely observed since their first discovery offshore Nova Scotia [1,14]. Pockmarks are usually formed as a consequence of gas and/or porewater eruption, most often followed by a period of unknown duration of recurring fluid escape. They often occur along continental margins commonly linked to subsurface structural and/or depositional features, including faults and salt diapirism in several settings [15–17], which reinforce fluid escape. Pockmarks have also been identified

in shallow waters, including semi-enclosed shallow embayments and even in lakes [18,19] and lagoons, as well as in deep water environments [20,21].

The distribution of pockmarks has commonly been linked to faults that constitute very important active conduits for fluids to migrate to the surface [22–26]. In many regions, single pockmarks, composite pockmarks and pockmark strings have been observed above faults and weakness zones in soft sediments, providing vertical pathways for migrating fluids. In the Black Sea, gas venting is abundant along canyon walls and is strikingly linked to the fault outcrops [25]. The pockmark field in the Gulf of Cork, Ireland, is formed by enhanced gas flux from an underlying fault system [4]. In Arctic fjords, faults and igneous sills play an important role in channelling fluid flow and forming pockmarks with high density [9]. In the Barents Sea, most of the pockmarks can be associated with leakage pathways through a shallow fault system or along inclined bedding planes [27]. Pockmark size is also related to sediment thickness. In the Belfast Bay field, small and shallow pockmarks occur in thin sedimentary sequences, while large ones occur in thicker sequences [28]. The Holocene sediment thickness is positively correlated with the pockmark sizes of Passamaquoddy Bay [29].

The normal activity of the pockmarks may be interrupted by occasional gas-escape events [30]. Many studies have reported a relationship between pockmark activity and earthquakes [30]. Any large ground-shaking event, such as an earthquake or large landslide, could cause interstitial gas bubbles to be suddenly expelled into the water column [31]. Seabed fluid flow may occur in advance of earthquakes or be triggered by earthquakes. Earthquakes trigger gas venting from the seafloor in areas with high seismicity, such as in Northern California [32], Sea of Marmara, Turkey [33–35] and the Arabian Gulf [36]. In areas with low seismicity (Vancouver Island), long-term seepage monitoring showed no correlation between fluid escapes and seismic events [37]. The non-systematic correlation between seepages and seismicity may be attributed to either small magnitude earthquakes being unable to cause fluid mobilisation [38] or dispersed seismic energy in the area [37]. The pockmark field of Patras Gulf is an example, where pockmark activity has been reported as a precursory earthquake phenomenon from the Patras earthquake in 1993 [39]. The same field exhibited strong evidence of activation at least twice—during two major earthquakes of magnitude 5.4 and 6.4 R on July 14th, 1993 and June 8th, 2008 [39,40]. For this reason, Judd and Hovland, in their book "*Seafloor Fluid Flow*", mentioned that: "*The pockmarks off Patras, northern Peloponnesus, Greece, represent some of the most spectacular and best-documented events in active pockmarks*" [30] (pages 230–231).

The Patras Gulf pockmark field (PGFP) is located in the southeastern part of the Patras Gulf in the vicinity of the city of Patras (Figure 1a). The site has been under investigation since 1996 [39–42]. Although the pockmark field has a long history of marine geophysical investigations, the data acquired from specific parts of the field are sparse and fragmentary and do not allow a complete, detailed and in-depth knowledge of the field. The major findings of the past marine geophysical surveys were that the field consists of numerous craters (72 in number) of variable shapes and extents, limited to an area of about 2.5 km^2. Fifteen sediment cores collected within the PGPF showed that the surficial sediments consist of fine materials, mud and silt with low sand content [43].

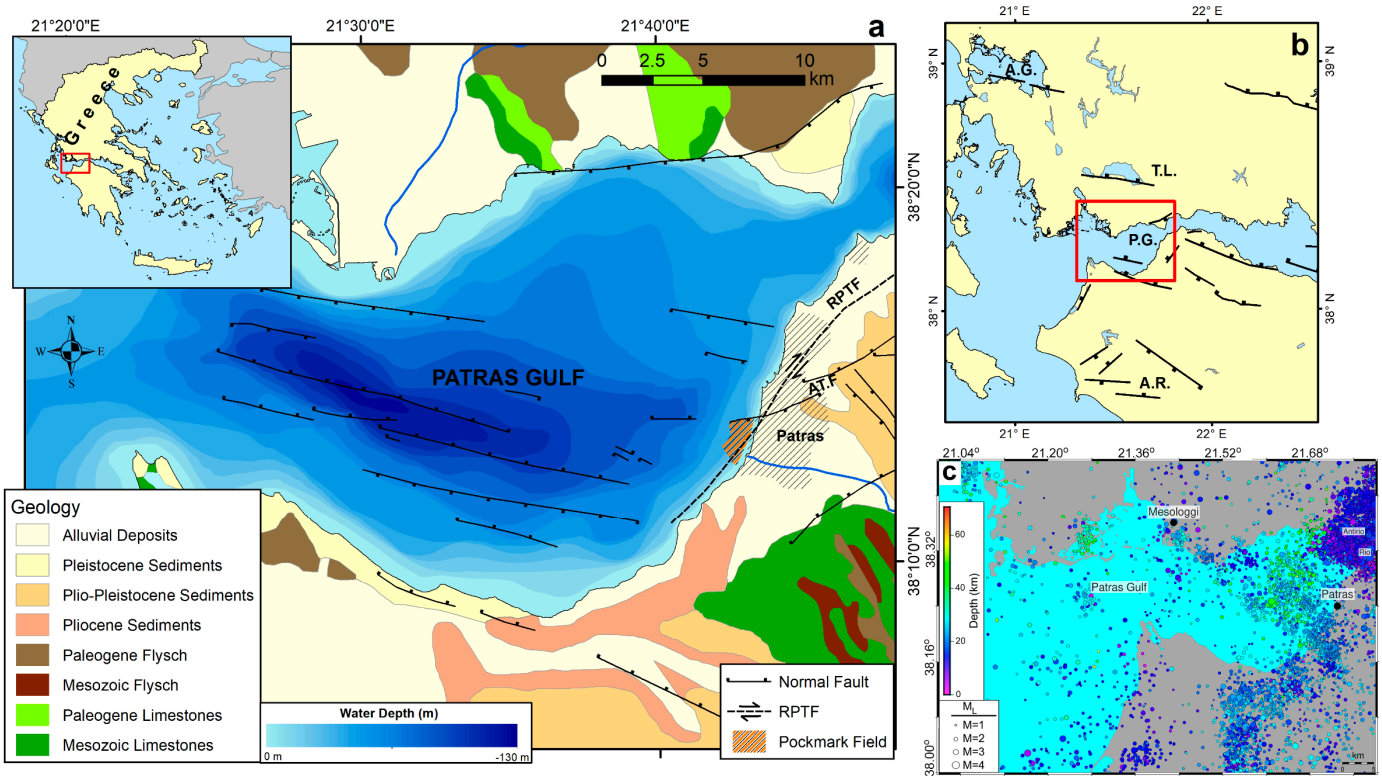

Figure 1. (**a**) Simplified geological map of Patras Gulf showing the major faults in the area and the location of the pockmark field; index map of Greece showing study area. (**b**) Tectonic map of Western Greece, (Geological data from [44]; Fault data from [45]) (AT.F: Agia Triada Fault; RPTF: Rio-Patras Transfer Fault; P.G.: Patras Gulf; A.G.: Amvrakikos Gulf; T.L.: Trichonida Lake; A.R.: Alfios River). (**c**) Seismicity map of Patras Gulf (Earthquake location data were retrieved from NOA-IG [46]. The color scale depicts depth distribution of the epicentre of the events).

Through years of repeated surveying of the area, in conjunction with the application of more precise and sophisticated marine remote sensing techniques, new aspects regarding the configuration of the area are constantly revealed. Within the long history of the investigation, the PGPF has been altered. From 1997 to 2015, within the area of the pockmark field, the new Patras harbour was built, and a significant part of the field was heavily modified. A number of pockmarks have been totally or partially covered by filling materials for the construction of the breakwater and the docks of the new harbour.

In this paper, we present the new findings of the PGPF as revealed through detailed and systematic surveying, utilising modern marine sensing techniques, including multi-beam, chirp sub-bottom profiles and dual frequency side-scan sonar, operated following a dense grid of tracklines. The data cover gaps in information from previous surveys. Synthesising and comparing newly acquired data and similar data from previous surveying, we aim to present the spatial distribution of the pockmarks, define the seismostratigraphy of the field and the migration of the gas through the sediments strata, ascribe possible modifications in the configuration of the PGPF through time and investigate the link between the PGPF and the tectonic activity of the area. Furthermore, the origin of the seeping gas was assessed using isotopic analyses.

1.1. Regional Setting

Patras Gulf is a semi-closed gulf which is open to the Ionian Sea on its western side and is linked through the Rio-Antirio strait to the Gulf of Corinth on its eastern side. Patras Gulf is the western part of the Patras-Corinth rift zone. The bathymetry of the gulf is controlled by linear structures (extensive active faults) trending WNW–ESE, which are the result of the

geological setting that characterises the gulf area (Figure 1a) [47–50]. The southern flank of it is controlled by the major faults and the northern by antithetic and synthetic faults, forming an asymmetric graben with the north-dipping major listric fault [50]. The WNW-trending faults are presently active, as revealed by the recent seismicity in the area, and exert a strong geomorphologic control on the landscape, including river courses (e.g., Alfios River), lakes (e.g., Trihonis Lake) and the shallow gulfs of Patras and Amvrakikos (Figure 1b) [45].

The graben seems to terminate against the ENE–WSW normal faults controlling the Plio-Pleistocene sequences outcropping onshore in the SE part of the Gulf. A NE–SW trending fault system called the Rion—Patras fault zone also controls the Patras rift zone [48]. The pockmark field is located at the intersection of WNW–ESE, ENE–WSW and the NE–SW fault zone. The evolution of the Gulf of Patras during the Late Quaternary is the consequence of the interaction between active tectonic subsidence (3–10 mm/yr), high sedimentation rate (2–3 mm/yr) and global sea level rise [50,51]. High-resolution profiles showed the existence of two layered sequences through the Gulf of Patras. The upper, attributed to the Holocene [50,51], is almost transparent and overlies the lower sequence that contains strong parallel to sub-parallel reflectors. The highly reflective surface on the top of the lower sequence is attributed to the basal unconformity of the Gulf, which is associated with the Last Glacial Maximum (~21 ka) and the early part of the following transgression (Late Pleistocene) [50,51] when the low sea level (~120 m below present level) most probably disconnected the gulf from the Ionian sea and the gulf became subaerial exposed. Surficial sediments mainly consist of silt and clay with low amounts of sand—except in the areas near the Rio-Antirio straits and the deltas at the northern part of the Gulf [51].

Western Greece is one of the most seismically active areas in the Mediterranean [52]. The Patras Gulf generally represents lower seismicity compared with the high seismicity of the Rio-Antirio strait, while the central and western parts of the gulf show a seismicity gap [49]. The spatial distribution of the earthquake epicentres for the time interval 2011–2022 shows medium seismicity in the eastern part of Patras Gulf, low in the central and western part and high in the Rio-Antirio strait (Figure 1c).

1.2. Previous Studies—Pockmark Field Activity

The pockmark field is at the southern end of the coastal zone of the city of Patras, in the wider area of the new Patras harbour. The activity of the field has been recorded in at least four phases since 1993. The results of these recordings are provided briefly in the following text.

1.2.1. Activation Due to the 5.4 R Earthquake of 14 July 1993

The first recording of the PGPF and its relation to earthquake activity was in 1993 [39]. An increase in seawater temperature of about 6.2 °C (from 16.8 °C to 23.0 °C) was recorded 10 m above the seabed prior to an earthquake of 5.4 R, which occurred on 14 July 1993, with the epicentre located 6 km ESE from the pockmark field [53,54]. The increase in temperature, observed in three time snaps, was associated with gas emissions from the field. Additionally, it was observed that at least nine pockmarks were still venting gas bubbles three to four days following the earthquake. All these pockmarks were in the northern sector of the field where the Agia Triada Fault (AT.F) dominates the area (Figure 1a). In a survey that took place 40 days after the earthquake event, no evidence of gas flares was recorded, suggesting that the activation of the field had ceased. The increase in seawater temperature was considered an earthquake precursor [39].

1.2.2. In-Situ CH_4 Measurements

Between 2002 and 2003, monitoring of the PGPF activity was attempted by operating a methane sensor (METS®,Franatech GMBH, Germany) above 14 pockmarks. Emphasis was given to the activity of one crater complex, called "P4", which showed high methane concentrations in the water near the seafloor during monitoring. Dissolved CH_4 amounts ranging from 3 to 707 nmol/L were recorded on a yearly basis, without showing any

seasonal patterns but displaying rather a spasmodic supply rate of CH_4 to the water column [41]. However, after a strong earthquake (4.7 R, 30 July 2003, 60 km east of the field), significantly higher dissolved methane concentration levels (420 to 1476 nmol/L) were measured near the seabed of pockmark 'P4'.

1.2.3. Gas Monitoring Module (GMM)

The emissions of pockmark P4 were investigated further in 2003–2004. Then, a cabled observatory, the Gas Monitoring Module (GMM), measured the gas and CH_4 seepage above the crater for 201 days, providing—for the first time—a data set of such extent from a gas-bearing pockmark [42,55]. Within the period of GMM deployment, more than 60 pulses of CH_4 increase were recorded. Increases in the dissolved methane concentration create a series of events that usually begin and end with changes in the physical properties of seawater. The most intense escapes are characterised by a sharp drop in seawater temperature (T) and pressure (P). These CH_4 peaks are also associated with H_2S peaks. This seepage fluctuation, which is associated with T-P drops, can be attributed to an active process driven by gas pressure built up in the pockmark sediments and/or as a passive effect driven by oceanographic (e.g., upwelling) and morphological factors (e.g., T-P drops caused by turbulence and Bernoulli-type effects induced by sharp depressions) [42]. During the periods of operation of the GMM, in the wider area, a number of small seismic events occurred (M < 4, except for one event). A comparison of the observatory data with the seismological data was performed for earthquakes > 3 R that occurred within a radius of 30 km from the point location. Five events out of fifteen were slightly correlated with gas seepages, as indicated by the slight increase in dissolved methane concentration [41].

1.2.4. Activation by the 6.4 R Earthquake of 8 June 2008

So far, the last recording of the PGPF activity was obtained in June 2008, when an earthquake of 6.4 R occurred at Movri, 32 km SW from the field [56].

Repeated side-scan sonar surveys conducted 2, 3, 4 and 15 days after the major earthquake revealed pockmarks that had been activated, as indicated by gas flares on the sonographs [40,41]. The spatial distribution of those flares did not show any geographical pattern within the field. The number and intensity of the gas flares showed a gradual decrease over time.

2. Materials and Methods

2.1. Marine Geophysical Survey

Bathymetric mapping of the study area was performed with a 180 kHz multibeam echosounder (MBES) (Elac Seabeam 1185). This system operates with 126 beams, and it was motion-compensated by an SMC IMU-108 motion sensor. An RTK GNSS was used to achieve < 10 cm lateral positioning accuracy. Sound–velocity profiles were acquired using a Valeport Midas CTD, and the sound velocity at the transducers was continuously measured using a Mini-SVS. Data acquisition was made through Hydrostar v.3 software and Hypack 2014 Suite. Processing was managed with Hysweep 2014 software. All grids shown in this paper have a cell size of 1 m, except when specifically mentioned otherwise. In the areas where the breakwater was constructed, data from a very dense trackline network using a single beam echosounder were used (Elac Nautic Hydrostar 4300, Kiel, Germany), which were acquired before the establishment of the harbour breakwater.

High-resolution sub-bottom profiles were acquired using a Kongsberg Geoacoustics Geopulse Plus sub-bottom profiler system with a Universal transceiver, an acquisition display, and an over-the-side Transducer Mounting (array of four transducers) with a hydrophone. The operating frequencies ranged between 1.5 and 11.5 kHz, which achieved greater penetration with a maximum vertical resolution of 10 cm. Chesapeake Sonarwiz v.6 software was used for processing sub-bottom profiles and extracting acoustic types, reflectors and thicknesses.

An Edgetech dual Frequency (100 and 400 kHz) digital towfish 4200SP with an Edgetech 4200-P topside Processor Side-Scan Sonar system was used for emitting and acquiring the two frequencies simultaneously. Moga Software SeaView v.5.1.49 was used for processing and producing side-scan sonar mosaics.

A dense network of 14 tracklines was acquired, running parallel to the shoreline with a line spacing of 100 m. Furthermore, 46 lines were acquired, running perpendicular to the above (Figure 2). The total length of the grid tracklines was about 90 km.

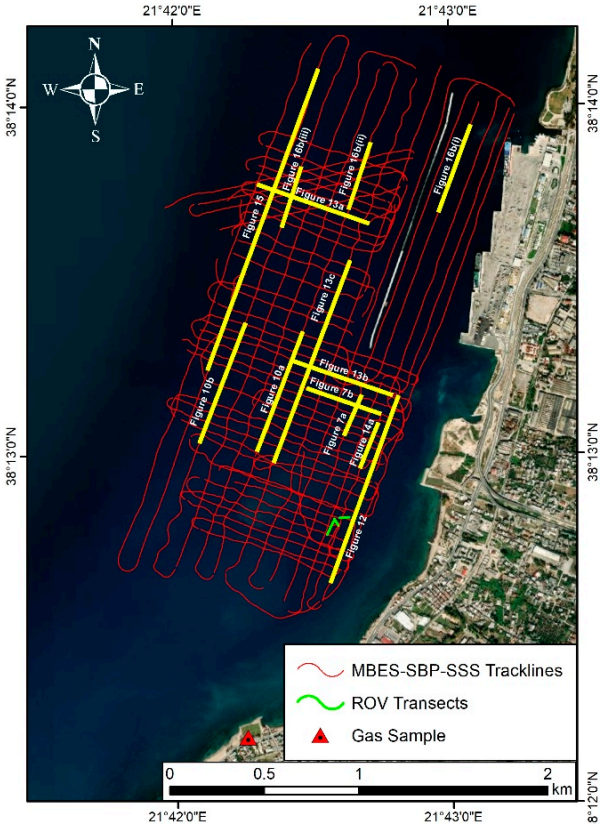

Figure 2. Map of the survey area showing the geophysical survey tracklines, ROV transects and the position of the well where gas samples were collected; yellow thick lines indicate the location of seismic profiles presented in the paper.

A ground-truthing survey was carried out in selected pockmarks using a Subsea Tech Guardian mini-ROV equipped with an underwater position system (USBL, Blueprint Subsea SeaTrac). In total, 3 ROV dives were conducted inside selected pockmarks and on the seafloor outside the pockmarks and photographs and videos were collected.

The analogue geophysical data (3.5 kHz sub-bottom profiler and Side-Scan Sonar) acquired in the previous surveys [39,42,57] was converted to digital and was reprocessed to be comparable with present data. Furthermore, we compared the profiling data with the core sediments retrieved from five drillings from the study area [58].

2.2. Gas Analysis

Groundwater and gas samples were collected from a well on the shore next to the pockmark field (Figure 2). The area was selected after performing a microseepage flux survey by the closed chamber method in the coastal zone of Patras near the pockmark field (unpublished data). The water and gas samples were stored in 200 mL and evacuated 100 mL glass bottles, respectively, and sealed with silicone septa and aluminium caps. All samples were analysed at Isotech Labs Inc. (Champaign, IL, USA) for C1-C6 hydrocarbons, He, H_2, Ar, O_2, CO_2, N_2, using a Carle AGC 100–400 TCD-FID GC with accuracy and precision 2% (1σ)) and stable C and H isotopic composition of CH_4 (δ^{13}C-CH_4, δ^{2}H-CH_4,

using a Finnigan Delta Plus XL mass spectrometer with precision ±0.3‰ (1σ) for ^{13}C, ±4‰ (1σ) for ^{2}H).

3. Results

3.1. Pockmark Field

3.1.1. Pockmark Distribution, Size and Shape

Multibeam bathymetric data revealed the presence of numerous seabed depressions, which make up an impressive pockmark field (Figure 3). The field covers a well-delimited area of 2.4 km^2 between the 17 and 45 m isobaths. The use of the MBES led to the accurate and complete mapping of the pockmarks in comparison to the previous surveys, where the mapping was based on the use of the single beam echosounder and sparse datasets of sub-bottom profiler and side-scan sonar [39–42,57]. The number of pockmarks obtained in the present study was ninety-two (92), which occupy an area of 0.41 km^2, approximately 20% of the entire extent of the field, which is much higher than the seventy-two (72) pockmarks obtained previously [42,57]. Twenty-three (23) out of the seventy-two (72) previously recorded pockmarks are now completely buried under the breakwater and the docks of the new harbour (Figure 3). Moreover, the comparison of the datasets showed that three (3) pockmarks identified and mapped in the present study were wider and have been partially covered. This finding increases the number of the field's pockmarks to 115—92 well-formed and 23 completely covered by the harbour installations.

The pockmarks, according to their morphological characteristics, can be distinguished into three main morphological classes (Table 1):

- Unit pockmarks: they have a diameter of 8 to 20 m, and their relative depth, compared to the surrounding seabed, varies from 1 to 5 m. They are small in size, and they could be considered early stages of development (Figure 3a,c).
- Normal pockmarks: they are circular or ellipsoidal in plan view, the diameter ranges from 20 to 130 m, and their relative depth reaches 14 m. These pockmarks can be characterised as being in a mature stage of development (Figure 3a,d).
- Composite or complex pockmarks: they have an irregular shape in plan view, their size is large and reaches a perimeter of 805 m, and their relative depth reaches up to 20 m. They are pockmarks that resulted from the amalgamation of neighbouring normal and unit pockmarks (Figure 3a,e).

The geographical distribution of the pockmarks, both well-formed and covered by the harbour construction, shows that the field can be divided into two main sectors of about the same seafloor extent (~1 km^2) (Figure 3a). Though the average spatial density of the total field is 50 pockmarks/km^2, the northern sector includes 55 pockmarks, while the southern sector includes 31 pockmarks, suggesting a higher density of pockmarks in the northern sector of the PGPF in relation to the southern one. Furthermore, the number of pockmark occurrences is higher south of AT.F and at the shallow part of the southern sector (Figure 3a; HD1 and HD2, respectively). The northern limit of the pockmark field is very well-delimited and corresponds to the offshore continuation of the active fault of Agia Triada (see also Section 3.1.5). Surprisingly, six small pockmarks were recorded further to the north of the AT.F lineament, which has never been reported in the previous surveys. The assumption that these pockmarks developed in the last 15 years seems rather weak, and their recording should be attributed to the best resolution systems in the present survey. Within the field, the pockmarks appear to form "clusters" (Figure 3d), which are usually collinear "chains" (Figure 3f). Collinear pockmarks may occur for several hundred meters. A large pockmark, or the joining of two, may occur at the end of such "chains" of pockmarks (Figure 3).

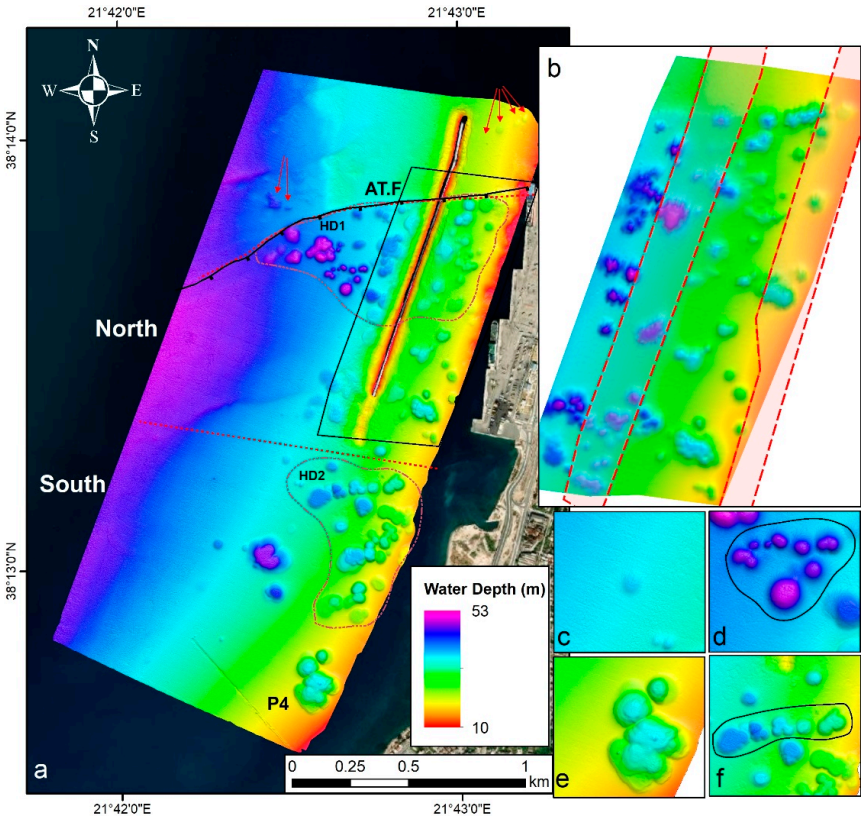

Figure 3. (**a**) Bathymetric map of the PGPF. The map also shows the location of Agia Triada Fault (AT.F) and the location of the largest pockmark 'P4'. Dotted red lines separate the two sectors (North and South) of the pockmark field and delimit areas of high pockmark density (HD1 and HD2); red arrows indicate the location of the pockmarks north of AT.F discovered in the present study. (**b**) The bathymetry of the PGPF before the construction of the harbour was derived from single beam data (cell size 2.5 m). The dashed polygons delineate the areas of PGPF covered by the harbour installations. (**c**–**f**) Detailed bathymetry showing (**c**) unit pockmarks; (**d**) a cluster of normal and small composite pockmarks deliminated by black line; (**e**) the largest composite pockmark of the field; (**f**) a pockmark ''chain'' of linearly arranged pockmarks deliminated by black line.

Table 1. Descriptive measurements of the PGPF pockmarks.

	Total	**North Sector**	**South Sector**
Total Number	92 (+23 buried)	55 (+23 buried)	31
No of Unit Pockmarks	9	4	3
No of Normal Pockmarks	54	35	15
No of Composite Pockmarks	29	16	13
Diameter (m) min–max (mean)	8–260 (72)	8–200 (65)	12–260 (90)
Perimeter (m) min–max (mean)	25–806 (218)	25–637 (207)	38–806 (260)
Volume (m^3) min–max (mean)	165–360,682 (22,247)	165–97,094 (15,102)	181–360,682 (38,654)
Relative Depth (m) min–max (mean)	1–19.3 (7.3)	2.5–15.3 (7)	1–19.3 (8.7)
Slope (degree) min–max (mean)	5–46 (26)	5–46 (26)	6–41 (29)
Relative Depth—Diameter ratio min–max (mean)	0.03–0.47 (0.13)	0.03–0.47 (0.14)	0.04–0.26 (0.11)
Circular	37	23	8
Elliptical	55	32	23

Descriptive measurements for the 92 pockmarks are summarised in Table 1. All over the PGPF, the pockmarks are 7.3 m on average, deeper than the surrounding seafloor, while there are pockmarks up to 20 m deep. Most of the pockmarks have been formed between 20 and 43 m water depth, and their occurrence shows an almost moderate correlation (R = 0.4) with the seafloor depth. However, the larger pockmarks exhibit a tendency toward greater depths of water (Figure 4a).

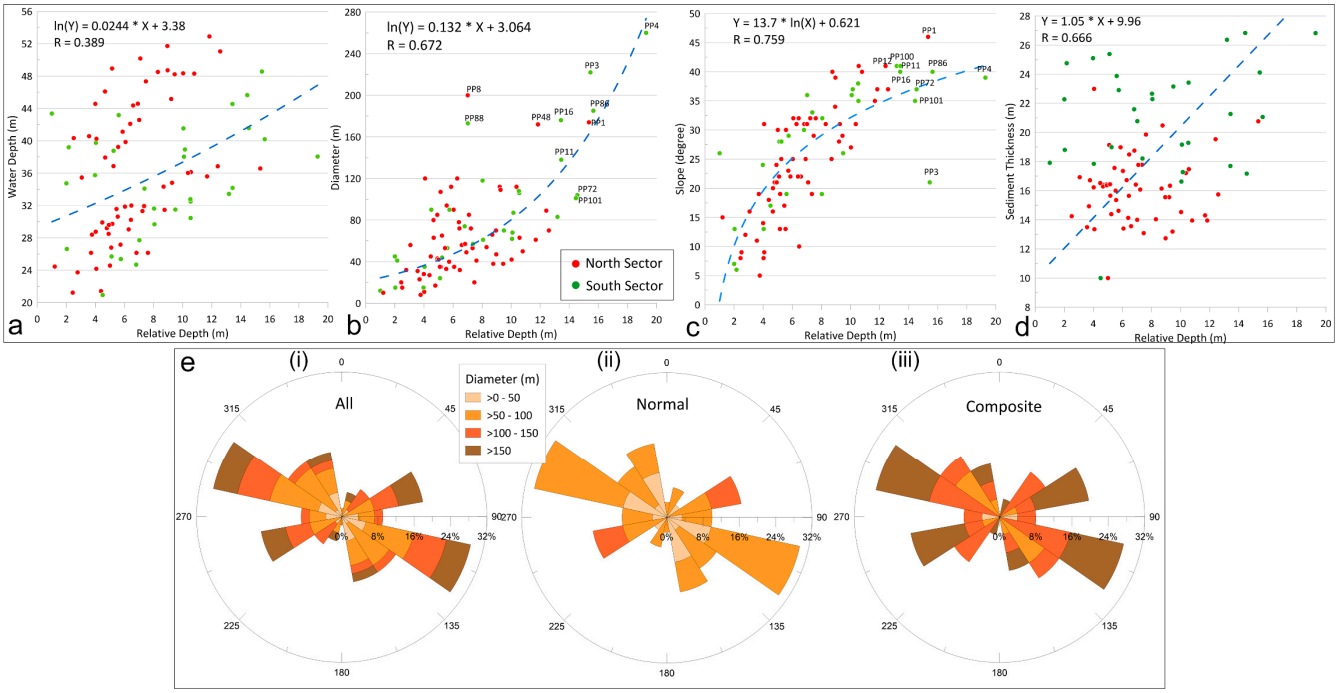

Figure 4. Diagrams of (**a**) water depth vs. pockmark depth; (**b**) diameter vs. pockmark depth; (**c**) slope vs. pockmark depth; (**d**) sediment thickness vs. pockmark depth; (**e**) Rose diagram displaying the orientation of the pockmarks' long axes ((**i**): all pockmarks; (**ii**): normal pockmarks and (**iii**): composite pockmarks). The orientation of the axes has been grouped by 30 degrees.

Most of the pockmarks extend for less than 8000 m^2; the deepest and most extended pockmarks are usually found in the southern sector of the field. Over 60% of the pockmarks have a perimeter between 100 and 300 m, and the mean field diameter is 72 m. The relation between pockmark depth and rim diameter is strong (R = 0.67), suggesting that most are not scale-dependent features (Figure 4b). A similar correlation has been observed in the Belfast Bay pockmark field [28].

The seafloor slope of the PGPF ranges from 5° to 46°, with the low values (1.5°) corresponding to the background seafloor and the maximum values (up to 46°) to the pockmark sidewalls (Figure 4c). The mean sidewall slope is 26° and is much higher than other pockmark fields (e.g., Belfast Bay [28]).

There is a significant positive relationship between the sidewall slope and the relative depth, with the wider pockmarks showing steeper slopes (Figure 4c). In PGPF, pockmark side walls are usually steeper than the proposed angle of repose for submarine sedimentary deposits, which ranges between 20° [59] and 12.5–17.5° [60].

The mean volume of the pockmarks is 22,247 m^3, with the smallest pockmark approximately 165 m^3 and the largest 360,682 m^3. Based on the difference between present-day bathymetry and a hypothetical bathymetric model without the pockmarks, the total volume of the PGPF is estimated to be about 2.1 × 106 m^3, suggesting that a large volume of sediments has been displaced by the pockmark activity.

An analysis of the directions of the major axes of the ellipsoidal pockmarks showed that these are not randomly oriented (Figure 4e). The orientations of both normal and

composite pockmarks show an almost bimodal distribution, with the long axis having a prevailing WNW to ESE and WSW–ENE direction (Figure 4e).

Side-scan sonar revealed that the seafloor in the area is characterised by low reflectivity, which indicates the presence of fine-grained sediments. Optical data acquired from the present work, as well as from previous studies, together with the results from sedimentological analyses from previous studies (i.e., [43]), further supports this observation. Patches of very high reflectivity, suggesting coarse-grained sediments, are also recorded and were attributed to dumping material. The pockmarks recorded clearly on the sonographs have a characteristic acoustic pattern consisting of an acoustic shadow followed by a strong reflection, similar to other relative sonographs worldwide [30] (Figure 5a).

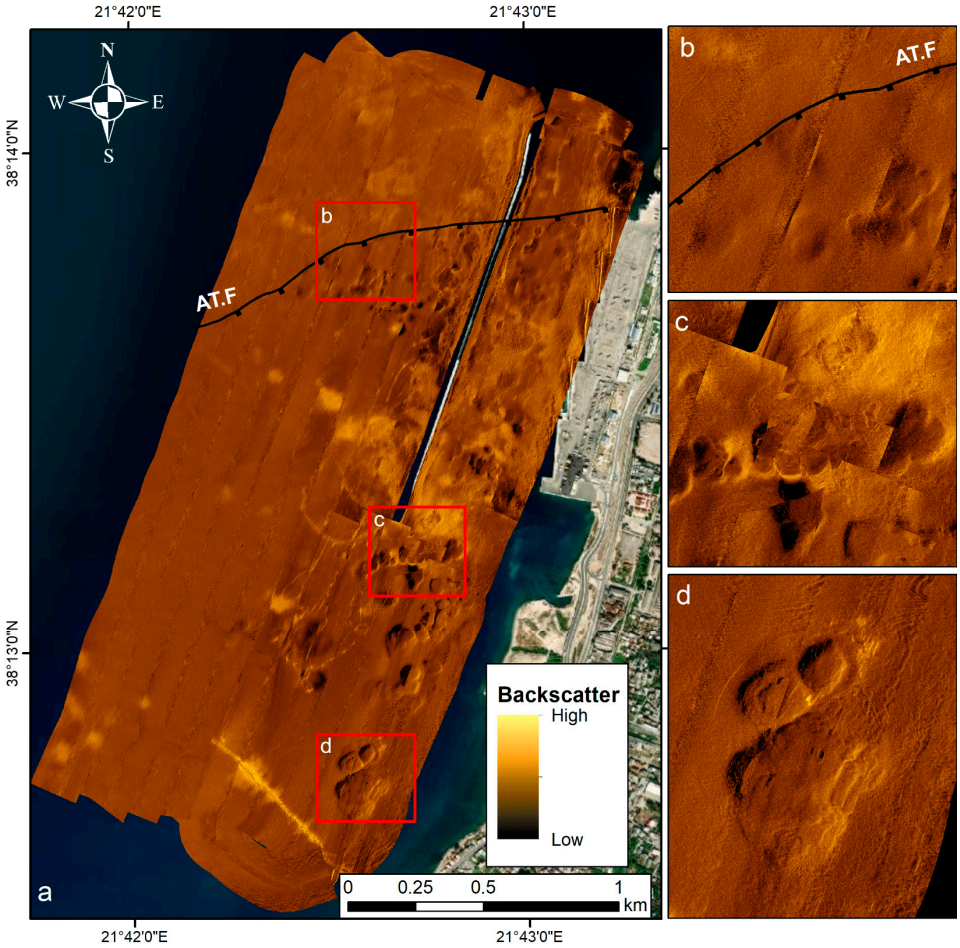

Figure 5. (**a**) The 100 kHz side-scan sonar mosaic of the PGPF area. Sonographs showing (**b**) pockmarks near Agia Triada Fault (AT.F); (**c**) a string of circular and composite pockmarks; (**d**) the largest composite pockmark of the field.

The backscatter intensity within the pockmarks appears slightly lower compared to the surrounding seafloor of the area, suggesting that the floor and the wall of the pockmarks area are covered by even finer sediments (Figure 5). The high backscatter values recorded on the rims of the pockmarks are attributed to the angle of incidence of the acoustic waves rather than to the coarser texture of the sediments (Figure 5).

ROV data showed that the floor of the pockmarks is composed of fluid mud. Toward the centre, small holes, 10–20 cm in diameter, were observed (Figure 6).

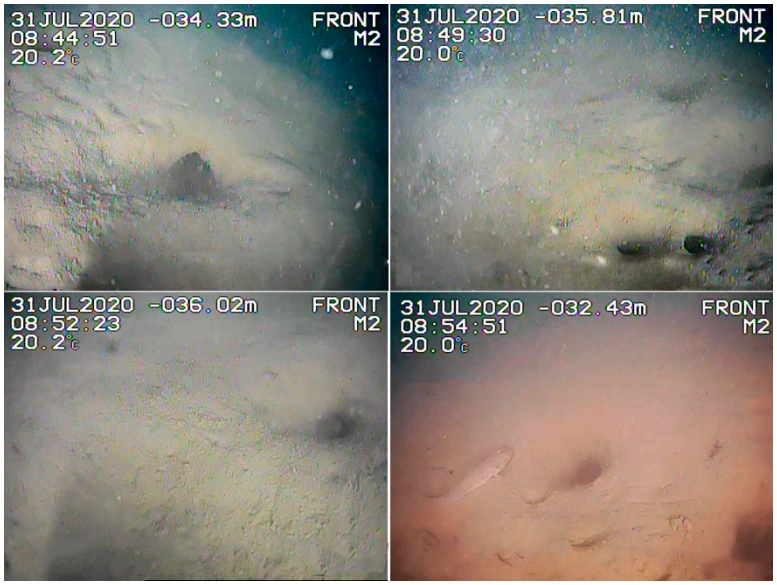

Figure 6. R.O.V. photos recovered inside selected pockmarks, showing the presence of small holes (diameter about 10–20 cm) in the muddy cover of the pockmarked floor.

3.1.2. Seismostratigraphy

The study of the seismic profiles generally showed the existence of two seismic sequences (SS). The upper one, SS I, is an almost acoustically transparent sequence consisting of low amplitude, almost parallel internal reflections. SS I overlies SS II, which is recorded as a single or a series of subparallel high-amplitude reflectors. Beneath SS II, no further penetration of the acoustic waves was achieved (Figure 7). The top reflector of SS II is attributed to the Pleistocene/Holocene boundary [16,39,50,51,57].

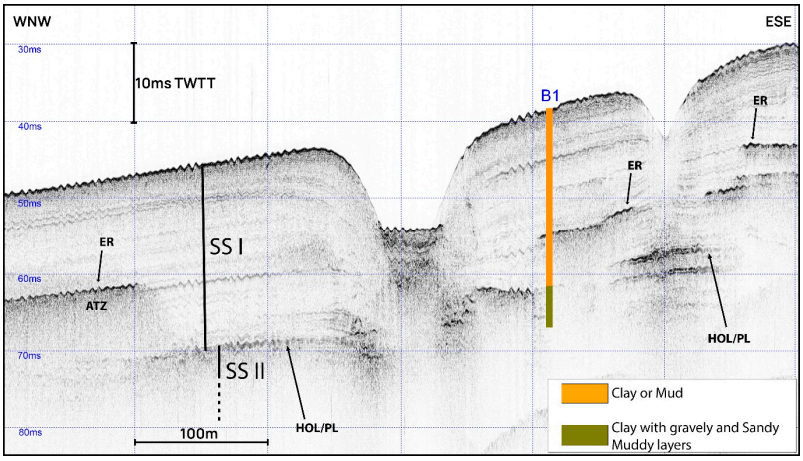

Figure 7. High-resolution seismic profile showing a typical stratigraphic pattern of the area consisting of two seismic sequences (upper SS I and lower SS II). The sedimentological interpretation of the well drilling [58] is superposed on the seismic profile (ER: Enhanced Reflector; ATZ: Acoustic Turbid Zone; HOL/PL: Holocene Pleistocene boundary; TWTT two-way travel time).

This highly reflective surface may be due to the large change in the geotechnical properties of the sediments, including the possibility of variations in the fluid content. Indeed, sedimentological analyses performed on the sediments from SS I and SS II showed lithological and geotechnical differences between the seismic sequences. The marine sediment samples were retrieved from five drillings conducted within the study area for the construction of the new harbour of Patras [58]. Based on the analysis, the upper sequence (Holocene, SS I) consists of clays with local interlayers of sandy muds, while the

base of the sequence (top of Pleistocene, SS II) consists of compacted clay with interlayers of gravels, sandy muds and biogenic clusters. In the later sediment facies, abrupt changes in the geotechnical properties of the sediments (hydraulic index from >100% to 85%, SPT from 2 to 5) were measured. On the other hand, the frequent presence of acoustic patterns related to gas accumulation in the sediments (i.e., Seismically Turbid Zones, Enhanced Reflectors) (see Section 3.1.3) at the top of SS II and locally in the lower part of SS I, together with the large number of pockmarks recorded in the SS I, strongly suggest the presence of fluids at the Pleistocene/Holocene interface, which locally migrated to the SS I. Based on the above, the abrupt change in geotechnical properties, together with the presence of gas-charged sediments on the profiles, suggest that the Pleistocene/Holocene boundary is a gas accumulation horizon.

The thickness of the SS I (Holocene) varies from 2 to 34 m (Figure 8). An abrupt increase in Holocene sediment thickness is observed south of the lineament of AT.F (Figure 8). The majority of the pockmarks have been observed in areas where the thickness of the SS I ranges from 12 to 20 m. Only a few pockmarks are obtained in areas where the thickness of SS I is more than 22 m (Figure 8). However, there is a strong relation (R = 0.67) between the pockmark depth and the thickness of the Holocene sequence (SS I), suggesting that the largest pockmarks have been formed in thick sediments (Figure 4d).

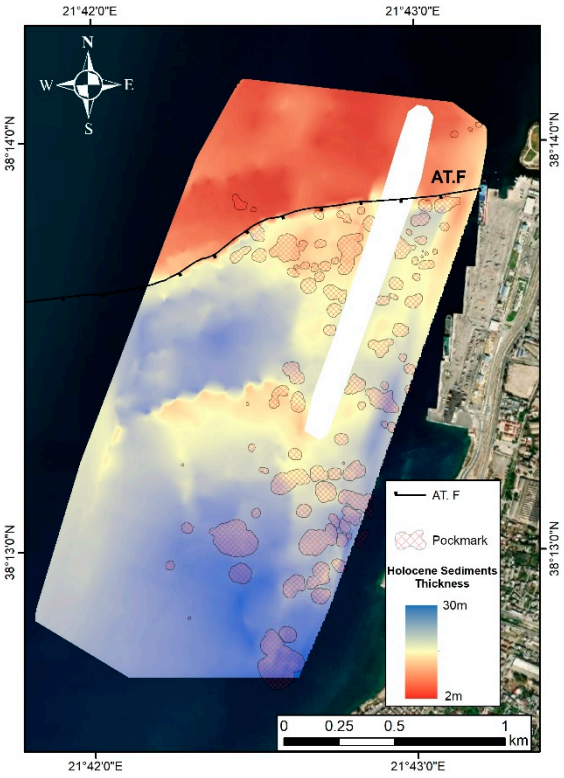

Figure 8. Holocene sediment thickness map of the PGPF. The thickness was derived under the assumption that the bottom is smooth without the presence of pockmarks.

Based on the thickness of the upper sequence, the acoustic characteristics of the seabed and the type of the deeper strong reflector, five distinct acoustic types [61] were defined. The spatial distribution of the acoustic types is shown in Figure 9.

Acoustic Type 1 (AT1) consists of an SS I with few, low amplitude and parallel internal reflections, which locally appear acoustically transparent overlying a sequence of parallel high-amplitude reflectors (SS II). Acoustic characteristics indicative of gas are absent in the SS I, suggesting that the gas has probably been accumulated in the Holocene/Pleistocene boundary and has not migrated upwards (within SS I). AT1 is mainly observed in the northern sector of the field, and its spatial distribution correlates well with increases in the Holocene sediment thickness (Figures 8 and 9).

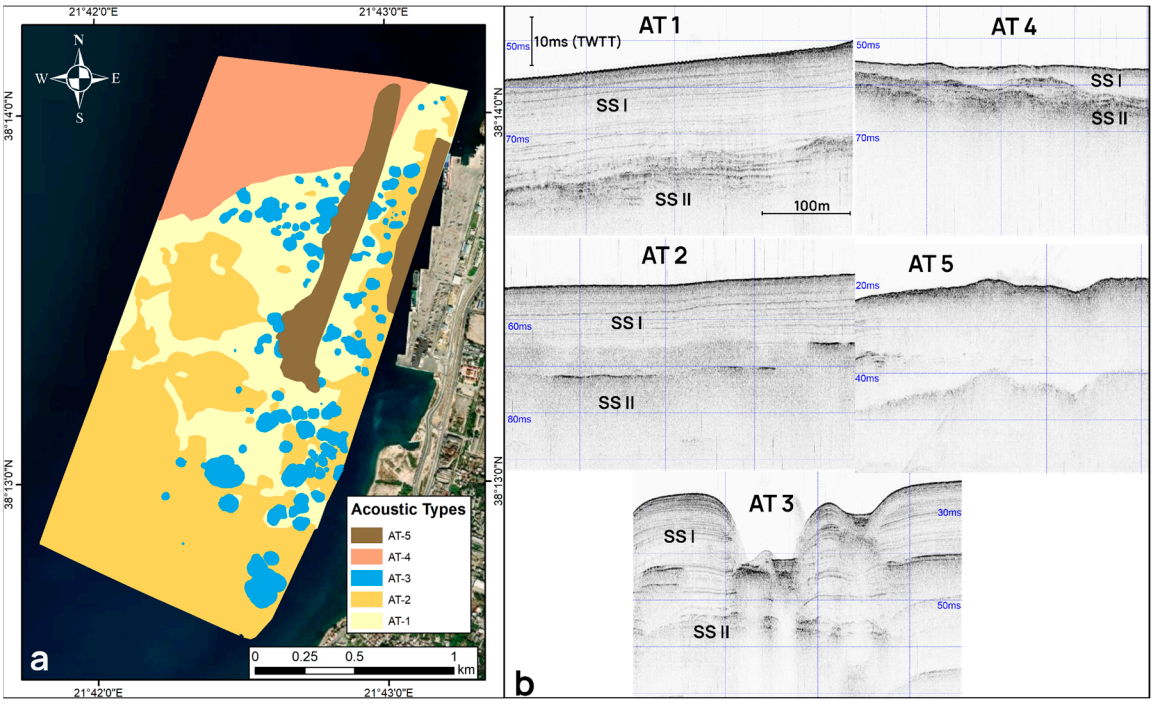

Figure 9. (**a**) Map of PGPF showing the spatial distribution of the acoustic types. (**b**) Representative seismic profiles of each Acoustic Type (AT) recognised by a high-resolution sub-bottom profiler (TWTT two-way travel time).

Acoustic Type 2 (AT2) is similar to AT1, but in AT2, the SS II is usually not visible due to the presence of high-amplitude reflectors and/or ATZs in the lower part of the SS I. Moreover, Enhanced Reflectors (ER) and Intrasedimentary Gas Plumes (IGP) have been recorded within the upper sequence. Locally, where the acoustic signal penetrates the upper sequence, the Pleistocene/Holocene boundary is characterised by a single high-amplitude reflector. AT2 is observed in the shallow part of both sectors and deeper off the pockmark field and also coincides well with the increased Holocene sediment thickness.

Acoustic Type 3 (AT3) is a specific acoustic type and represents pockmarks. It is characterised by a columnar disturbance, which is obtained below the bottom of the pockmarks and abruptly interrupts the parallel seismic reflections of the upper sequence (I) around the pockmark. Its geographical distribution is delimited to the pockmark location.

Acoustic Type 4 (AT4) consists of an almost transparent SS I with very few low-amplitude reflections overlying SS II, which is recorded by high amplitude and prolonged reflectors. In AT4, the thickness of the SS I is always lower than that of AT1 and AT2. AT4 is delimited to the northern part of the area and further north of the AT.F, which constitutes the southern limit of the acoustic type.

Acoustic Type 5 (AT5) is characterised by a very prolonged surface reflector with no sub-surface reflections or locally weak ones. AT5 is bounded peripherally by the harbour's breakwater and docks and represents disturbed deposits of coarse sediments related to its construction.

3.1.3. Gas in Marine Sediments

The study of the seismic profiles showed the existence in the area of various 'abnormal' acoustic characters, which are direct and indirect evidence for the presence of fluids in the sediments. The most frequently occurring acoustic characters are the Acoustic Turbid Zone (ATZ) (Figure 10a,b) [16,30,62–65] and Enhanced Reflectors (ER) (Figure 10a,b) [30,64–66]. Rarely, Intrasedimentary Gas Plumes (IGP) (Figure 10b) [62,63] and Seabed Doming (D) (Figure 10b) [64,67] were observed.

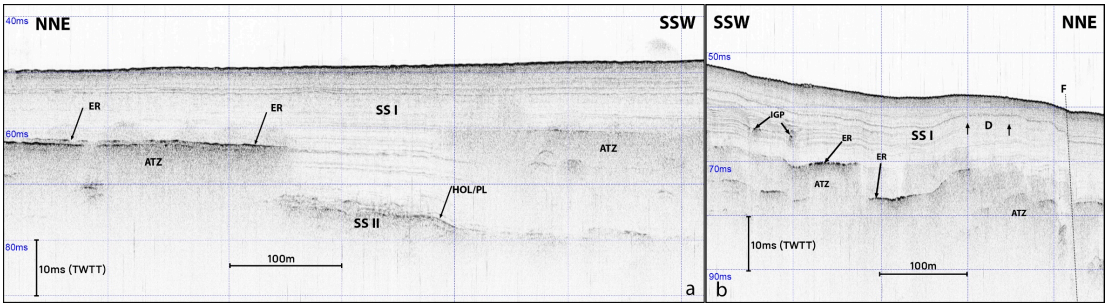

Figure 10. Representative high-resolution seismic profiles (**a**,**b**) showing the presence of Enhanced Reflectors, Acoustic Turbid zones, Intrasedimentary Plumes and Seabed Doming due to gas migration to the upper seismic sequence (I). (ER: Enhanced Reflector; ATZ: Acoustic Turbid Zone; IGP: Intrasedimentary Gas Plumes; D: Seabed Doming; F: Fault; HOL/PL: Holocene Pleistocene boundary; TWTT two-way travel time; SSI: upper seismic sequence; SSII: lower seismic sequence).

The most extended gas-related acoustic character observed in the seismic profiles is that of ATZ. These zones result from the attenuation of acoustic energy by the presence of gas bubbles within the interstices of the sediments. The gas front, which is the top of ATZ, shows up as a single strong reflection or as a combination of Enhanced Reflectors, indicating the upward migration of the gas (Figure 10).

Enhanced reflectors (ER) appear as coherent high-amplitude reflections with abrupt terminations. They have been observed in various stratigraphic levels in the SS I, suggesting the upward migration of gas (Figure 10). In many cases, Enhanced Reflectors are above the top of the ATZ or inside the ATZ (Figure 10).

ATZs are a widely spread acoustic character in the pockmark field and are mostly found below pockmarks in both sectors of the field (Figure 11a). Exceptions are the two limited areas (A and B) with a total lack of ATZ and ER; area A is located at the southern end of the northern sector, and area B is at the central part of the southern sector (Figure 11b). The Pleistocene/Holocene boundary has been clearly identified in both areas.

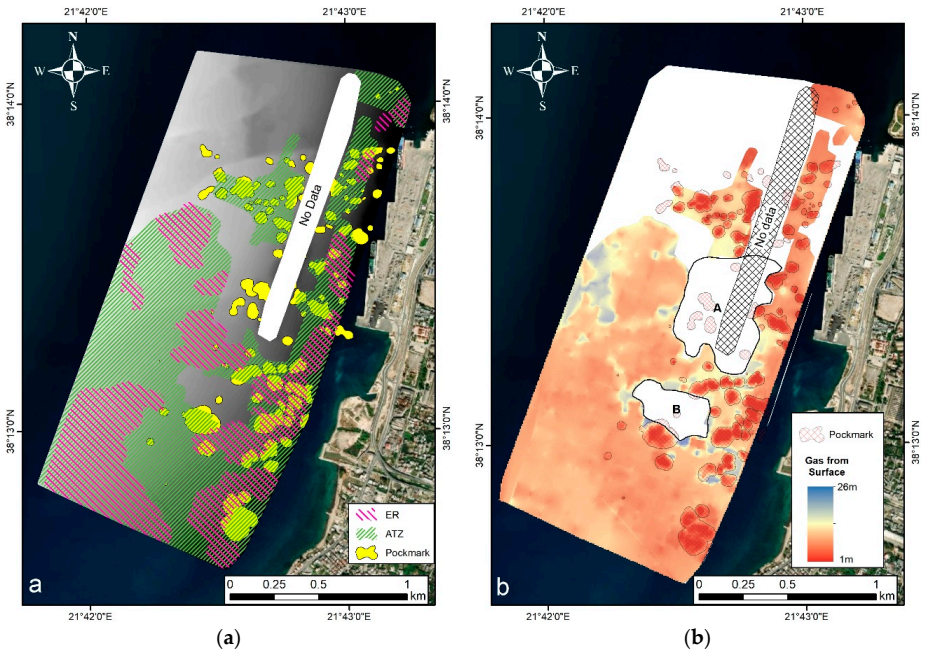

(**a**) (**b**)

Figure 11. (**a**) Map showing the spatial distribution of Acoustic Turbid Zones (ATZ) and Enhanced Reflectors (ER) and their relationship with the presence of pockmarks. (**b**) Map showing the depth below the seabed where the top of ATZ and ER has been recorded. A and B delimitate areas without ATZ and ER.

In general, it seems that the pockmarks are formed in the shallowest parts of the area where ATZ and ER have both been observed (Figure 11a). The pockmarks at the northern sector, at the proximity of AT.F, are solely linked with ATZ since a lack of ER is observed (Figure 11a).

3.1.4. Pockmarks Venting

In the seismic profiles, the pockmarks show acoustic characters indicative of their formation mechanism and activity. Profiles have shown that the common pockmarks are U- or V-shaped and abruptly interrupt the low amplitude internal reflections of the SS I (Figures 12, 13 and 14a). Some of them have a flat bottom and resemble a truncated cone. In many cases, the pockmarks were recorded with lateral reflections overlapping each other, creating synclinal or bow-tie structures, suggesting very steep slopes and narrow floors at the pockmark sites (Figure 13). Steep slopes seem to be affected by gravitative mass movements, as indicated by small, detached blocks that partially infill the pockmarked floor (Figures 12 and 13b). The floors of the pockmarks are always in the upper seismic sequence (SS I), as all pockmarks terminate above the base of the Holocene unit.

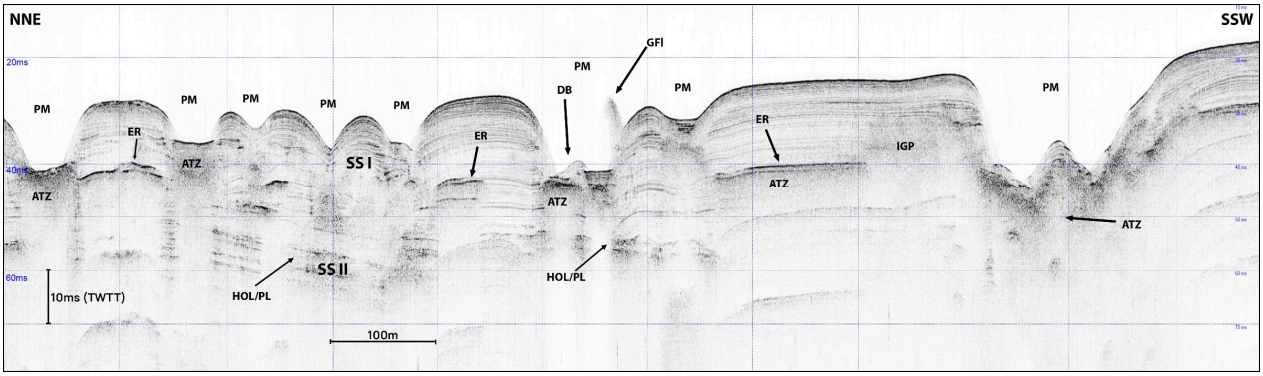

Figure 12. High-resolution seismic profile showing numerous normal and composite pockmarks, as well as the biggest pockmark in the field (right), located near the southeastern part of the study area. ATZs are found immediately beneath the majority of medium- to large-sized pockmarks. Above one of the pockmarks, a gas flare is recorded. The HOL/PL boundary is partially visible when the gas-related reflections in the upper seismic sequence disappear (PM: pockmark; ER: Enhanced Reflector; ATZ: Acoustic Turbid Zone; IGP: Intrasedimentary Gas Plumes; GFl: Gas Flare; DB: Detached Block; HOL/PL: Holocene Pleistocene boundary; TWTT two-way travel time).

On the profiles of the pockmarks, the ATZs are often present below their floor, suggesting that the sediments below the pockmarked floor contain gas and thus the potential for a continuous supply of gas from the Pleistocene/Holocene interface upwards to the pockmarked floor (Figures 12, 13 and 14a).

In some unit pockmarks, the continuation of the ER is abruptly interrupted just below the pockmarks floor (Figure 13b,c). This interruption of ER proposes gas escape through a weakness zone and, thus, the formation of small pockmarks. In some cases, a zone with a transparent acoustic character is observed below the pockmark floors and at their sidewalls (Figure 13c). The recording of this acoustically transparent zone probably indicates that: (i) the escape of fluids was not limited only by the bottom of the pockmark but also from the entire surface of the pockmark walls and (ii) the gas seepage was vigorous and disturbed the structure of the sediments. Similar processes have been reported by [39] in a pockmark of the field.

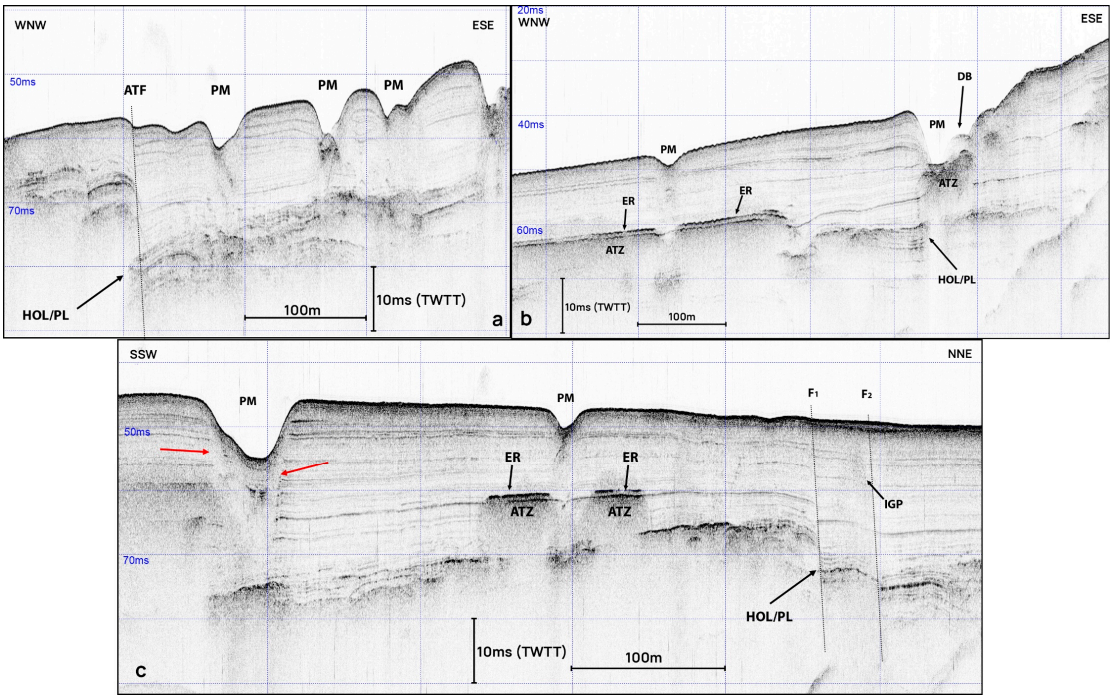

Figure 13. High-resolution seismic profiles showing (**a**) pockmarks with narrow floor on the north sector of the field near AT.F; (**b**) two pockmarks, a composite (right) in which the Acoustic Turbid Zone is close to the seabed and a Detached Block is recorded at the sidewall and a normal one (left) where ER and ATZ are interrupted below it; (**c**) a large pockmark (left) where a transparent acoustic character (indicated by red arrows) is observed under its floor and; an Intrasedimentary Gas Plume (right) located between two minor synthetic normal faults and a small pockmark (centre). (PM: pockmark; ER: Enhanced Reflector; DB: Detached Block; ATZ: Acoustic Turbid Zone; AT.F: Agia Triada Fault; HOL/PL: Holocene Pleistocene boundary; TWTT two-way travel time).

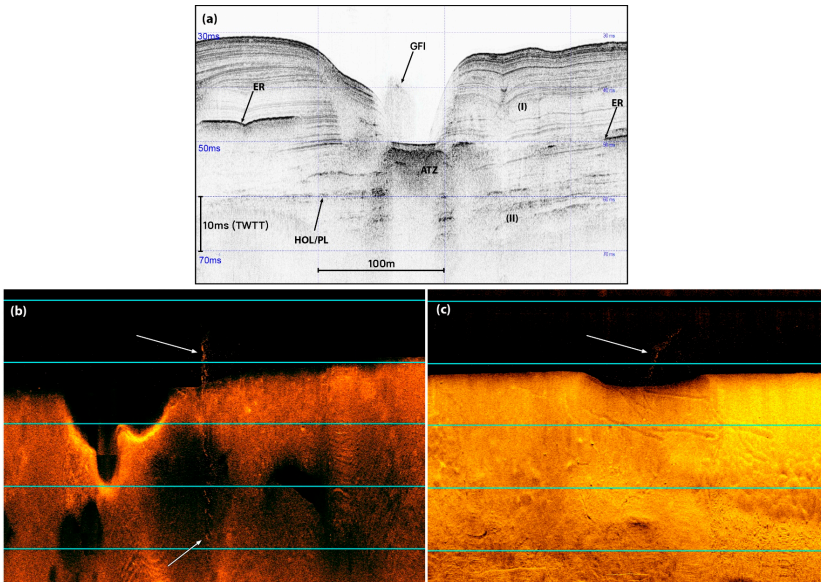

Figure 14. (**a**) High-resolution seismic profile showing a gas flare over a pockmark (ER: Enhanced Reflector; ATZ: Acoustic Turbid Zone; GFl: Gas Flare; HOL/PL: Holocene Pleistocene boundary; TWTT two-way travel time); (**b**,**c**) slant range uncorrected 400 kHz side-scan sonar sonographs showing gas flares (white arrows indicate their position) in the water column rise from the centre of the pockmarks (horizontal lines every 20m).

Few acoustic anomalies consisting of straight and inclined reflections were observed in the water column (Figures 12 and 14). These disturbances are located directly above pockmarks and have been recorded both on side-scan sonar sonographs and seismic profiles (Figure 14).

In the sonographs, there is a sharp, intense, and continuous pattern from the centre of the pockmarks to the sea surface, while the seismic profiles present a more diffuse acoustic character. Although side-scan sonar is typically used for mapping seafloor morphological features, the system has also been successfully used to track ascending bubbles from the seafloor to the surface [34,68–71]. Acoustic anomalies—due to the presence of gas bubbles in the water column—are usually referred to as 'gas flares', as suggested by Greinert et al. [68], to distinguish them from the 'plumes' that are defined as water column volumes with high concentrations of dissolved gas [72]. In high-resolution seismic profiles (e.g., CHIRP, 1.5–10.5 kHz), gas flares are also detectable, showing an almost vertical and dark smearing acoustic character [73].

The acoustic anomalies observed above Patras field's pockmarks were interpreted as gas flares due to active seepage of gas from the pockmarks. The 100/400 kHz side-scan sonar used in the survey is capable of detecting bubbles greater than 0.006 cm in diameter in 20 m and deeper waters [74]. During repeated surveys in periods with no earthquake activity, gas flares were observed in only a few pockmarks located at the northern sector of the field. The acoustically imaged gas flares extend in the water column from the seafloor to the sea surface, suggesting a continuous flow rather than a pulsing nature [75].

3.1.5. Active Faulting in the Pockmark Field

Active faults were identified from lateral displacements on reflectors in the high-resolution seismic profiles and from linear seafloor displacements in multibeam data. Integration of bathymetry and seismic profiles allowed measurement of fault orientation, dip, vertical displacement (fault throw) and fault activity.

Faults were picked line-by-line on seismic profiles and clustered into two groups: (1) "major" faults that appear in many seismic profiles, showing a sufficient displacement of the Holocene/Pleistocene boundary and can be correlated to bathymetric features and (2) "minor" faults that appear locally in few seismic profiles without bathymetric expression (Figures 15 and 16). In total, six normal faults were recorded in the area.

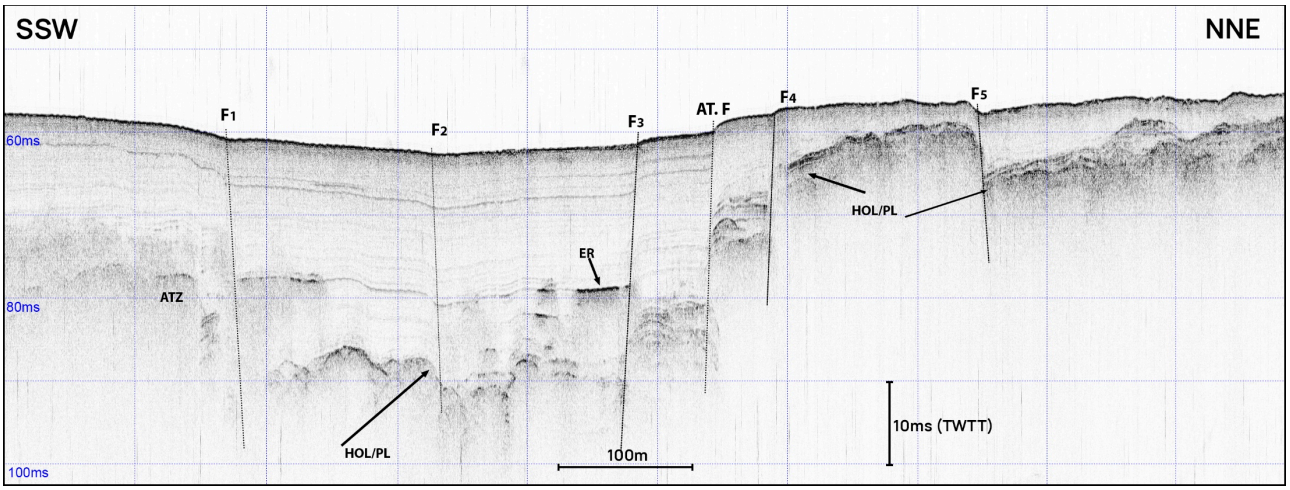

Figure 15. High-resolution seismic profile showing six normal faults that affect the structure of the layers. Enhanced Reflectors and Acoustic Turbid Zones are present in the upper sequence. (F: Fault; AT.F: Agia Triada Fault; ER: Enhanced Reflector; ATZ: Acoustic Turbid Zone; HOL/PL: Holocene Pleistocene boundary).

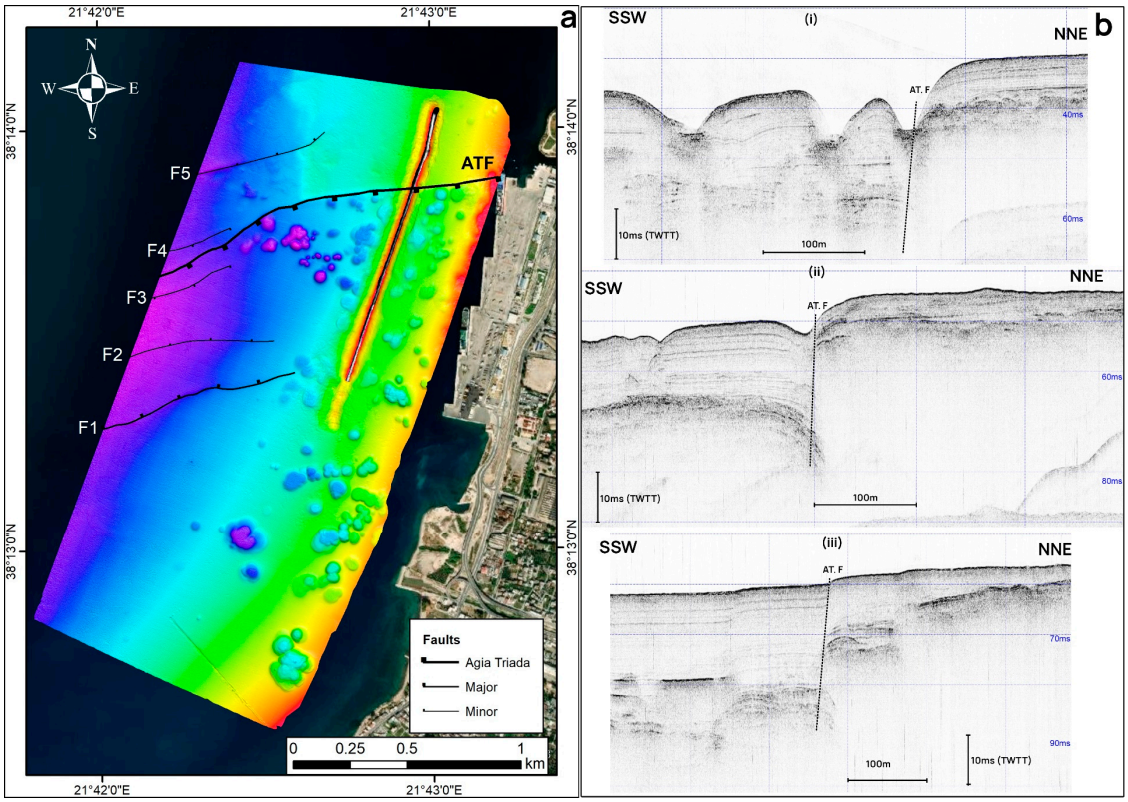

Figure 16. (**a**) Tectonic map of the pockmark field area. (**b**) Three seismic profiles parallel to the shoreline from shallow (**i**); medium (**ii**) to deep water (**iii**) showing the highest displacement, with a characteristic reverse drag on the hanging-wall block in the medium-depth seismic profile (AT.F: Agia Triada Fault; F: fault).

In the northern sector of the field, a group of linearly arranged pockmarks is located along the upper part of a slope with a bathymetric difference of 4 to 10 m. This "chain" of pockmarks has a WSW–ENE orientation and a length of about 1 km. Seismic profiles perpendicular to this slope revealed the trace of a WSW–ENE trending, south-dipping normal fault that causes a bathymetric difference of up to 5 m. The vertical throw of this normal fault, as measured by the offset of the Holocene/Pleistocene reflector surface, is about 15 m, with a small variation along strike. The thickening of the lithoseismic stratigraphy in the hanging-wall block of this fault, combined with the progressive decrease of the vertical displacement toward the surface, indicates its syn-sedimentary activity during the Holocene (Figure 15). This WSW–ENE striking normal fault is the offshore continuation of the AT.F that runs through the southern areas of the city of Patras [76–78].

At a distance of 750 m, south of the AT.F, an almost parallel topographic lineament occurred. Seismic profiles running perpendicular to this structure showed that it is located along the trace of a normal fault (F_1 fault in Figure 15) that causes deepening of the seabed bathymetry to the north. The dip of this normal fault decreases from west to east and does not affect the sediments near the coast. The vertical throw, as measured from the displacement of the Holocene/Pleistocene seismic surface west of the field, is about 12 m. This fault is antithetic to the AT.F, while it does not seem to continue toward the east near the coastline. Both faults, AT.F and F_1, fracture outcrop at the seabed and exhibit offsets that are clearly visible on a multibeam bathymetric map (Figure 3). A characteristic of this area is the arching of the Holocene sediments on the footwall block of this fault, possibly due to gas accumulations above the ATZ below.

A parallel, less extensive topographic lineament exists 250 m north of AT.F. Seismic profiles revealed another normal fault (F_5 in Figure 15) that dips to the north, forming a conjugate, divergent overlapping transfer zone with the AT.F. The throw measured from

the offset of the Holocene/Pleistocene seismic surface west of the field is about 5 m. This fault is also antithetic to the AT.F and F_4 fault, forming an uplifted horst-anticlinal structure (Figure 15).

In general, the study area is affected by an array of en-echelon normal faults with various degrees of overlapping, forming conjugate, convergent and divergent overlapping relay zones, depending on whether the faults dip toward the same or opposite directions, respectively [79]. Moreover, the area is affected by smaller faults, synthetic and antithetic to the above ones, that produce smaller topographic changes and smaller throws.

3.2. Methane Origin

The composition of the gas phase released from the water well located along the coast is reported in Table 2, and the CH_4 isotopic composition is shown in Table 3. The molecular composition of the gas shows that methane is the dominant component with a concentration exceeding 90 vol.% in the gas phase (and >80 vol.% in the gas extracted from the water by the head-space equilibration method). Heavier hydrocarbons (besides trace amounts of ethane) were not detected. The stable C and H isotopic composition of CH_4 ($\delta^{13}C$ and $\delta^{2}H$) is about −73‰ (VPDB) and −201‰ to −210‰ (VSMOW), respectively. This isotopic composition is typical of microbial origin (carbonate reduction) from the marine environment (Figure 17).

Table 2. Chemical analysis of gases (in vol %) in the samples of the coastal zone of Patras. In the water sample, the concentration refers to the gas extracted by head-space method using helium. The data are corrected for air contamination.

Sample	H_2S	He	H_2	Ar	CO_2	N_2	CH_4	C_2H_6	C_3H_8	iC_4	nC_4	iC_5	nC_5	C_{6+}
Water	bdl	-	bdl	0.23	6.22	9.55	83.99	0.0053	bdl	bdl	bdl	bdl	bdl	bdl
Air	bdl	bdl	bdl	0.08	1.9	5.54	92.48	0.0037	bdl	bdl	bdl	bdl	bdl	0.004

bdl = below detection limit.

Table 3. Isotopic analysis of CH_4 from the coastal zone of Patras.

Sample	$\delta^{13}C_{CH4}$ (‰, VPDB)	$\delta^{2}H_{CH4}$ (‰, VSMOW)
Water	−72.12	−201.3
Air	−73.93	−210.9

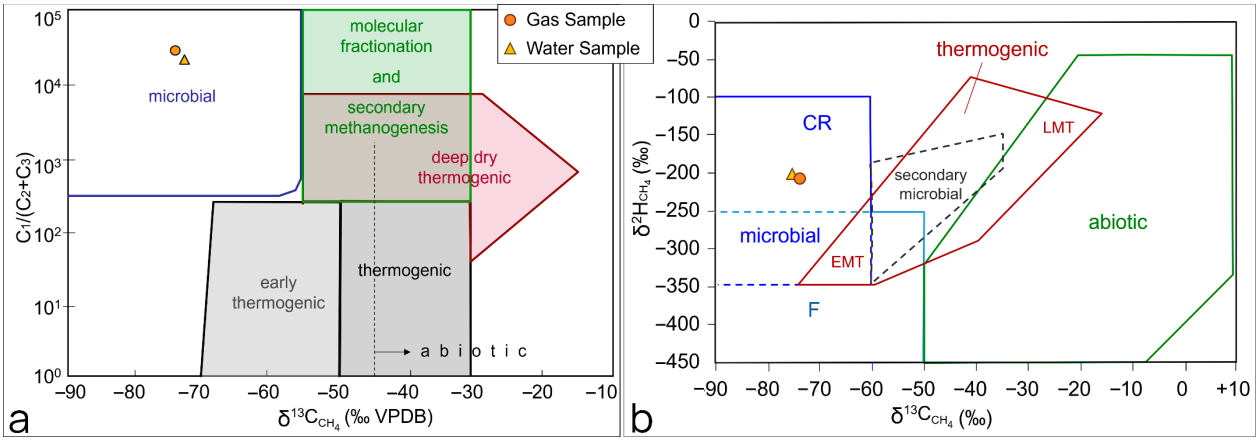

Figure 17. (**a**) Genetic diagram of $\delta^{13}C_{CH4}$ versus molecular composition of hydrocarbon gases (C1/ (C2 + C3)) (VPDB = Vienna Peedee Belemnite Standard) after [80]. (**b**) Genetic diagram of $\delta^{13}C_{CH4}$ versus $\delta^{2}H_{CH4}$ (CR: CO_2 reduction, F: fermentation, EMT: early mature thermogenic gas; LMT: late mature thermogenic gas) after [80].

4. Discussion

4.1. Pockmarks Spatial Distribution and Morphometry

A multidisciplinary survey consisting of high-resolution geophysical means and geochemical analyses provides new insights into the Patras Gulf Pockmarks Field (PGPF). In comparison to the 72 pockmarks recorded by the previous surveys [42,57], in the present study, 115 pockmarks were recorded, of which 23 were covered by the harbour installations. Although the formation of new pockmarks after the construction of the new harbour (in 2015) cannot be excluded, the difference in the number of pockmarks is likely attributed to the limitations of the previous studies (instrumentation and sparse tracklines). The application of morphometric measurements showed that the PGPF consists of pockmarks variable in size, ranging from small and well-defined (8 m in diameter and 1 m deep) to large (260 m diameter and 20 m deep) ones. Their mean diameter is 72 m, and they are, on average, 7.3 m deeper than the surrounding seabed. These measurements are comparable to relative datasets from pockmarks obtained in the Eastern Mediterranean and worldwide [15,27,81,82], though pockmarks can vary greatly in shape and size. The pockmark size dataset published by Picher et al. [81] shows a compilation of data reported in 57 published papers. The compiled dataset shows that the pockmarks are characterized by a wide range of sizes, covering more than four orders of magnitude, where most of the pockmarks are 10–250 m in diameter and 1–25 m deep. Their mean diameter is 128 m, and their mean depth is 9.6 m. Based on that, the pockmarks of PGPF fall well within the range of the above-mentioned mean sizes [81].

The pockmarks of the PGPF also present a variety of shapes. In total, three main classes (unit, normal and composite) and two dominant geometric shapes (circular and ellipsoidal) are attributed to the pockmarks, though the field is limited in extent. Similar observations previously made in other examined areas show that the pockmark shape variety should be attributed to different styles of formation—due to their activity history and underlying structural framework—rather than different sedimentary/ hydrographic characteristics, which can be considered constant within the pockmark field area [83,84].

The average density of the pockmarks in the PGPF is 50/km^2. Compared to the findings on other pockmark fields [84], the PGPF pockmark density (>5–10/km^2) is classified as 'hydraulically active'. This density is higher compared with 18 pockmark fields in the central North Sea, which ranges between 4 and 29/km^2 [85]. It is also higher compared to the East Breaks pockmark field in the Gulf of Mexico (<15/km^2) [15] and is similar to the Gulf of Maine (160/km^2) [30] but lower than Snøhvit hydrocarbon field in the SW Barents Sea (600–700 km^2) [27]. Moreover, the spatial density is not homogenous but appears higher in the northern section (55/km^2) (78/km^2, including the buried pockmarks) compared to the southern section (31/km^2). Hovland et al. [1] suggested that the development of the pockmarks depends on the established migration path, which has further dependencies on features like sediment thickness, strength, permeability and faulting. The density patterns in the PGPF agree well with that observation. The highest densities (up to 100 pockmarks per km^2) occurred at the proximity and southward of the AT.F, suggesting that the fault constitutes an important pathway for the upward gas migration in this field. Faults have been associated with fluid migration and seepages in the Barents Sea [27], Black Sea [25], Ireland [4], Marmara Sea [33–35] and Bohai Sea [26]. Furthermore, high pockmark densities (75/km^2) are also present in the shallow part of the southern sector. There, as well as in the previously mentioned high-density area, the Holocene sedimentary deposit thickness is low, and the depth occurrence of the ATZs is shallow, suggesting that despite the faulting, the number of pockmarks is also controlled by the sediment thickness (Figures 8 and 11). The density of the pockmarks in Belfast, Blue Hill and Passamaquoddy Bays is related to the thickness of the Holocene sediments, with the highest densities occurring in areas with thinner sediments [29].

The direction of the maximum axis of the ellipsoidal pockmarks and the collinear cluster of pockmarks ("chains" or strings) is of particular interest, as it may indicate the directionality of the hydrodynamic and endogenic processes controlling the formation

of the pockmarks [1,83,85,86]. The measurements in the ellipticity modes of the Patras pockmarks showed that the orientation of the major axes, in common and composite pockmarks, is not random but follows two main directions: WNW–ESE and WSW–ENE (Figure 4e). The WSW–ENE direction coincides well with the directions of the main local faults, suggesting that the fluids escaping along those faults play an important role in the field formation. This is further supported by the fact that the pockmark collinear clusters are found lined up in the same direction (Figure 3). The linear arrangement and the eccentricity of the pockmarks have commonly been linked to the underlying geological structure, whereby faults provide active conduits for fluids to migrate to the surface [87–89]. The other prevailing direction (WNW to ESE) shows an offset of about 20° to the faulting direction. This is probably due to gas escapes through other localised failures or along permeable horizons at the proximity of the faults since the Holocene clays are characterised by low permeability. A similar explanation has been given by other authors to explain the displacement of the pockmark appearance compared to underlying geological structures. Söderberg and Flodén [90] reported that pockmarks may not necessarily be located directly above a fault but can be formed in the peripheral parts of tectonic lineaments due to gas migrating sideways within the uppermost parts of the sedimentary strata. Webb et al. [91] attributed the displaced appearance of the pockmarks in the Oslofjord (Norway) relative to the underlying structural elements to the same mechanism. The arrangement of the PGPF seems to not be significantly affected by hydrodynamic processes. Although the occurrence of elliptical pockmarks in several fields has been attributed to the transport of sediments by seafloor currents during pockmark formation [85,92], the SW–NE direction of ellipticity, which is expected to be related to the direction of the prevailing currents, is extremely weak in all classes of pockmarks. This is in accordance with the weak SW–NE-trending bottom currents in the area [93].

The sidewalls of the PGPF pockmarks have slopes ranging from 2° to 48°, the steeper of which are observed mainly in the large pockmarks of the southern sector. The mean value of the slope (26°) is significantly higher than those in the Belfast Bay (8–12°) [28] and Oslofjord (13°) pockmark fields [91]. The steep sidewalls are unstable and thus often result in slumping [59,91]. Such gravitational movements have been found by acoustic imaging and direct observation in pockmarks with steep sides in the Gulf of Maine [94].

The PGPF pockmarks slope more than the proposed 20° angle of repose for fine-grained sediments [59]. This, together with the fact that the sediments of SS I are soft (clays with interlayers of sandy mud), suggest that the PGPF pockmarks with steep sidewalls are likely to be affected by sidewall slumping. At least two pockmarks from the southern sector exhibit evidence of wall slumping and partial infilling of the pockmarked floor (Figures 12 and 13b). On the other hand, steep sidewalls probably indicate that pockmarks are in some way active or are being kept clear of sediment. Kelley et al. [95] suggested that slopes exceeding the angle of repose were indications of pockmark activity. Audsley et al. [83] proposed pockmark depth more closely relates to activity status, with deeper pockmarks likely to have been active for longer periods of time or to have experienced a more intense venting of gas. Similarly, Webb et al. [91] interpreted the relatively deeper and steeper-sided pockmarks within the Oslofjord field to be recently active and wider shallower ones as older or inactive for a long time. Based on the depth–width ratio of PGPF, the large, deep and steep-sided pockmarks of the southern sector could be considered the most active area in the entire PGPF.

Side-scan sonar showed very low backscattering inside the pockmarks, suggesting that the pockmarks were infilled with muddy deposits. The low backscatter of the floor, walls and rims suggest that the Patras pockmarks generally lack carbonate clasts and chemosynthetic communities, which are usually associated with pockmarks. Carbonate clasts are recorded by high to very high backscatter amplitudes because of the strong differences in densities and acoustic velocities between the carbonate clasts and the surrounding mud and their small relief [96–98]. Moreover, methanotrophic communities (e.g., shells of chemosynthetic bivalve beds) contribute to enhancing the amplitude of the signal [99,100].

ROV images recovered from a deep, steep-sided pockmark of the southern sector of the PGPF confirmed the presence of fluid mud inside the pockmark and the absence of benthic ecosystems related to fluid seepage. The absence of such benthic ecosystems may be related to the fine-grained character of the sediments. Dando et al. [101] observed scarce fauna in the stiff clay at the base of a pockmark in the Fladen Ground area of the North Sea, while abundant megafaunal communities were observed inside several pockmarks of the North Sea with coarse-grained sediments on their floors [102]. A lack of benthic ecosystems related to pockmarks has also been reported [103] in a shallow water pockmark field (15–40 m) in the Bay of Concarneau (French Atlantic coast). Furthermore, in Inner Oslofjord, Norway, the analysis of macrofaunal assemblages inside and outside numerous pockmarks showed no influence on the composition of the fauna at any taxonomic level [104]. In the PGPF, the ROV inspection also showed the existence of small holes (10–20 cm in diameter) scattered on the muddy floor of the examined pockmark. Most probably, these holes result from bioturbation (e.g., benthivorous fishes), though the possibility that they are related to gas leakage should not be excluded.

4.2. Relation to Faults and Subsurface Characteristics

The northern sector of PGPF is affected by an array of en echelon normal faults. The faults exhibit various degrees of overlapping, forming conjugate, convergent and divergent overlapping relay zones, depending on whether the faults dip toward the same or opposite directions, respectively [79]. Moreover, the area is affected by smaller faults, synthetic and antithetic to the above ones, that produce smaller topographic changes and smaller throws. The Agia Triada fault (AT.F) delimits the field to the north, although few small pockmarks have been observed further north. This dense fault system and the associated weakness zones reinforced the formation and development of many pockmarks, recording the highest spatial density of pockmarks (80/km^2) in the northern sector and particularly at the proximity of the AT.F (100/km^2). Collinear clusters of pockmarks have also been observed, trending in the WSW–ENE direction, which coincides well with the direction of the faults. The good coherence in orientation between collinear pockmarks and faults further supports the close relationship between the regional structural setting and the local fluid escaped patterns, which, in turn, control pockmark configuration and spatial distribution. At similar sites where the structural setting dominates, a pockmark field configuration has been reported, such as in the Barents Sea [27], Ireland [29] and the Nasha Region of the South China Sea [105].

The PGPF also shows an affection for the Holocene sedimentary deposits (SS I), of which the thickness varies from 2 to 34 m (Figure 8). The strong correlation between the pockmark depth and the thickness of the Holocene sequence (SS I) suggests that the largest pockmarks have been formed in thick sediments (Figure 4d), like pockmarks in the Belfast and Passamaquoddy Bays [28,29].

Throughout the study area, many examples of upward gas migration have been detected in the marine sediments. Gas-related acoustic patterns mainly include Acoustic Turbid Zones (ATZs), Enhanced Reflectors (ER) and, to a lesser extent, Intrasedimentary Gas Plumes (IGP). All of them were recorded solely within the Holocene sequence (SS I) and constitute evidence for an upward gas migration from the Pleistocene/Holocene boundary, which can be considered a gas accumulation horizon. ATZs are a widely spread acoustic character along the PGPF except for two limited areas (A and B) at the southern end of the northern sector and at the central part of the southern one (Figure 11b). These areas exhibit an interesting difference in pockmarks appearance; area A is characterised by a cluster of pockmarks, and area B is characterised by an almost lack of pockmarks—apart from a very small one. This difference is probably attributed to a different upward-migrating gas status: (i) in area A, continuous upward migration of gas toward the floor of the pockmarks and total escape of gas and (ii) in area B, near absence of upward migration of gas except the formation of the small pockmark.

4.3. Pockmark Field Gas Origin

The gas analysis of the two samples from the coastal zone showed that the gas was mainly methane of microbial origin, produced by carbonate reduction (Figure 17a) in anaerobic marine sediments during organic matter mineralisation [106,107]. Methane of microbial origin is quite common in shallow, coastal waters, including deltaic environments [108], estuaries or coastal zones with mangroves [109], where there is enhanced organic matter supply.

The gas in the Patras Gulf could be the product of buried terrestrial organic-rich layers formed during sea-level lowstands. Patras Gulf is connected to the Ionian Sea through straits with depths less than 50 m, suggesting that during glacial periods, the sea level drops (up to 120 m below the present level) may have ceased the marine connection of the gulf with the open sea and—together with deltaic progradation of the major rivers flowing in the area [51,110]—may have led to accumulation of organic-rich sediments in the gulf. Chronis et al. [51] argued that the gas of Patras Gulf is the result of the buried organic-rich deposits during the last glacial/interglacial cycle. A similar pattern of gas production resulting from buried organic-rich sediments related to the last glacial sea-level lowstand and subsequent overlapping during the Holocene transition has been previously established for the pockmark field in the Bay of Fundy, eastern Canada [31]. In addition, the production of methane from buried organic-rich deposits formed during lowstands has been proposed to explain the microbial methane found in the Belfast pockmark field [94].

4.4. Pockmark Field Activation

The Patras pockmark field displayed strong evidence for activation at least twice during two major earthquakes of magnitude 5.4 and 6.4 R on 14 July 1993 and 8 June 2008, respectively [39,40]. Several pockmarks were found to be active for a few days after the 1993 earthquake, of which the epicentre was located near the pockmark field. Similarly, the field was activated by the 2008 major earthquake, which occurred 32 km SW of the field at the Northwestern Peloponnese. In both activations, the number and intensity of the gas flares showed a gradual decrease over time, in a period of 15 to 30 days. Post-earthquake pockmark venting has been reported in several places worldwide [30,32–36]. The long-term Gas Monitoring Module (GMM), which was deployed inside a composite pockmark of the southern sector, showed the normal behaviour of a pockmark during a period with no major earthquakes [55]. Gas seeps exhibit significant temporal variations in venting behaviour, and few studies have been conducted using visual census [111] or acoustic methods [112]. The GMM recorded 60 "pulses" of CH_4 increase, associated with T-P drops, in a period of almost six months, using an METS methane sensor [42,55]. Based on direct evidence and long-term monitoring data, the PGPF is characterised by a normal activity consisting of micro-emissions (1 event/3–4 days), which is interrupted by episodic and vigorous venting triggered by major earthquakes. The earthquake-induced vigorous venting seems to last for 15 to 30 days after the mainshock.

In the present study, acoustic flares (gas seepage) in the water column, immediately above a few pockmarks, have been detected for the first time during a period of calm seismic activity in the area. In addition to the seepage pulsation that has been recorded by GMM, the water column data indicate gas seepage above the pockmarks, implying ongoing pockmark activity. The acoustically imaged gas flares extend in the water column from the centre of the pockmarks to the sea surface, suggesting a continuously flowing—rather than a pulsing—nature [75].

Similar pockmark field behaviour has been reported by Baltzer et al. [103] in the Concarneau Bay pockmark field. Ongoing gas venting activity in the field could be due to the repetitive action of the short-term pressure-controlled process superimposed on longer-term temperature-controlled processes and episodically on earthquake occurrence.

The acoustic data collected from the water column above the pockmarks of PGPF after the mainshock of two major earthquakes (1993 and 2008) were reprocessed and plotted onto the new bathymetric map (Figure 18). The spatial distributions of gas flares triggered

by two earthquakes showed different patterns. The 1993 earthquake flares are concentrated in the northern sector of the field and at the proximity of AT.F. On the contrary, the 2008 earthquake flares are widespread over the entire field.

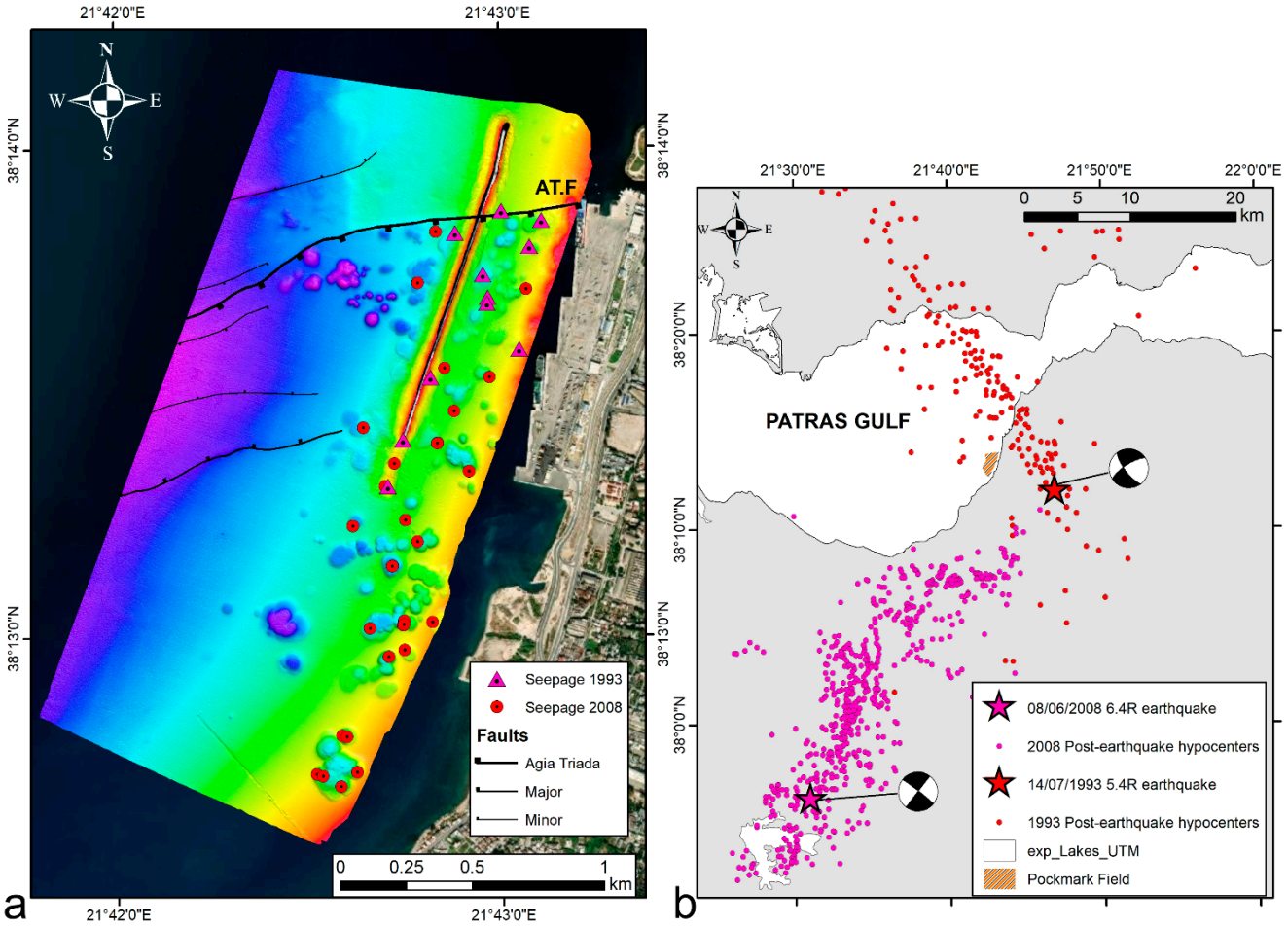

Figure 18. (**a**) Bathymetric and tectonic map of the PGPF showing the locations of seepages after the 1993 and 2008 major earthquakes which affected the field; (**b**) map showing the location of the epicentres of the two major earthquakes, their focal mechanism and the distribution of the post-earthquake events (earthquake data of 1993 from [54,113] and 2008 from [114]).

Although the earthquake mechanism in both events is similar (strike slip), the locations and distances of the epicentres of the main and post-earthquake events (Figure 18b) could explain the different spatial distribution patterns of gas flares in the PGPF obtained in these two seismic events. The 1993 Patras earthquake was located in the eastern city outskirts, roughly 6 km east of the pockmark field, at the city's harbour. The earthquake had a shallow depth (~10 km) and caused a complicated aftershock sequence that is described in detail by Tselentis et al. [115]. The aftershocks extended in a NNW direction to the north of Patras. The focal mechanism of the mainshock suggests a strike-slip fault, with one nodal plane in the NNW direction, i.e., similar to the aftershock sequence. Although of medium size, the event caused significant damage to buildings near the AT.F fault and activated the pockmarks localised near the AT.F's offshore extension. The Movri earthquake in 2008 (6.4 Mw) ruptured an NNE right lateral fault; its epicentre was ~30 km south of Patras [56,114]. The hypocenter of the event was rather deep at ~20 km, i.e., in the lower crust. The earthquake caused damage and triggered secondary phenomena in the epicentral area (e.g., rock falls, landslides) but did not significantly affect Patras's buildings. Thus, it seems that the earthquake was strong enough to induce cyclic loading in the uppermost

sediments of the PGPF area and consequently trigger upward gas migration and emissions from the entire field.

5. Conclusions

A multidisciplinary survey consisting of high-resolution geophysical means and geochemical analyses provides new insights into the Patras Gulf pockmarks field. This survey has not only revealed the existence of new pockmarks, but it has brought new knowledge regarding their spatial distribution and the level of activity, their link with the structural framework of the area, the fluid escape structures, the fluid pathways used, and finally the origin of the fluids.

High-resolution marine remote sensing techniques, including MBES, sub-bottom profilers, side-scan sonars and ROV, together with laboratory techniques, enabled us to record in detail the active pockmark field, which developed in Patras Gulf. In the past, the field showed co-seismic activation, while over the last 26 years, the field has been partially covered by the Patras city harbour.

The acquired data sets showed that:

- The main mechanisms for the development of the field are the local tectonism and the internal characteristics of the sedimentary layers.
- The local faulting appears to be the main contributor to the arrangement of the field, as it was shown to regulate the density, spatial distribution and geometry of the pockmark shapes in the field. All these morphometric characteristics are in line with the direction of the main active faults and the associated tectonic failures recorded in the region.
- The lithological parameters and the thickness of the upper sedimentary deposits in the examined area also contributed to the formation of the field. Thick, muddy deposits enhance the development of pockmarks in terms of quantity (high number of pockmarks) and sizes (large sizes) of pockmarks.
- Pockmarks recorded have steep sidewalls (up to 40°), suggesting recent activation. Steep slopes (at least >20°) seem to promote slumping events in the pockmarks. No acoustical or optical evidence of benthic ecosystems linked with gas seepages was recorded.
- The combined acoustic data sets detected, in detail, the migrated gas in marine sediments and the water column. The sediments provide evidence for the presence of gas by the recordings of Acoustic Turbidity Zones (ATZs), Enhanced Reflectors (ER) and, to a lesser extent, Intrasedimentary Gas Plumes (IGP). Evidence for the gas in the water column was revealed by the gas flare recordings.
- Geochemical analysis showed that CH_4 is the dominant component of the released fluid, and its isotopic analysis showed a microbial origin, which is common in shallow marine environments.
- Although the source of the gas flare pockmarks changes through time, the fact that gas flares are always recorded above the field denotes an ongoing pockmark activity.
- Through time, local and regional, active tectonic processes and possibly recent anthropogenic activities (construction of the harbour) alter the migration paths of the escaping gas and cause modifications in the growth of the field. The field serves as a living underwater landscape, which has the potential to respond directly to seismic activity, even as a precursory response to earthquakes.
- This study showed that multidisciplinary surveying, incorporating marine geophysical and laboratory investigations, can illuminate aspects of a pockmark field in relation to configuration, structure, activity and triggering mechanisms.

Author Contributions: Conceptualisation, D.C., G.P. and M.G.; methodology, D.C. and G.P.; formal analysis, D.C. and N.G. (Nikos Giannopoulos); investigation, D.C., X.D., S.S., E.F., N.G. (Nikos Georgiou), G.E., E.S., G.F., M.G. and G.P.; data curation, D.C. and G.P.; writing—original draft preparation, D.C., G.P., M.G. and S.K.; writing—review and editing, D.C., G.P., M.G., S.K., X.D., G.F.

and G.E.; visualisation, D.C. and N.G. (Nikos Giannopoulos); supervision, G.P.; project administration, G.P.; funding acquisition, G.P. All authors have read and agreed to the published version of the manuscript.

Funding: This research work was supported by the Hellenic Foundation for Research and Innovation (H.F.R.I.) under the "First Call for H.F.R.I. Research Projects to support Faculty members and Researchers and the procurement of high-cost research equipment grant" (Project Number: 4369) and by the Laboratory of Marine Geology and Physical Oceanography, University of Patras internal funds.

Institutional Review Board Statement: Not applicable.

Informed Consent Statement: Not applicable.

Data Availability Statement: Data available on request.

Acknowledgments: Many thanks to Dimitris Eleftherakis for his assistance in geophysical surveys and the captain and crew of Milady Myllord III for their help during the research cruises. Thanks to Metrica S.A. and HxGN SmartNet for providing GNSS RTK data. The authors would like to acknowledge the anonymous reviewers for their valuable comments, which helped to improve the quality of this manuscript.

Conflicts of Interest: The authors declare no conflict of interest.

References

1. Hovland, M.; Judd, A.G. *Seabed Pockmarks and Seepages: Impact on Geology, Biology and the Marine Environment*; Graham & Trotman: London, UK, 1988.
2. Harrington, P.K. Formation of Pockmarks by Pore-Water Escape. *Geo-Mar. Lett.* **1985**, *5*, 193–197. [CrossRef]
3. Whiticar, M.J. Diagenetic Relationships of Methanogenesis, Nutrients, Acoustic Turbidity, Pockmarks and Freshwater Seepages in Eckernförde Bay. *Mar. Geol.* **2002**, *182*, 29–53. [CrossRef]
4. Jordan, S.F.; O'Reilly, S.S.; Praeg, D.; Dove, D.; Facchin, L.; Romeo, R.; Szpak, M.; Monteys, X.; Murphy, B.T.; Scott, G.; et al. Geophysical and Geochemical Analysis of Shallow Gas and an Associated Pockmark Field in Bantry Bay, Co. Cork, Ireland. *Estuar. Coast Shelf Sci.* **2019**, *225*, 106232. [CrossRef]
5. Krämer, K.; Holler, P.; Herbst, G.; Bratek, A.; Ahmerkamp, S.; Neumann, A.; Bartholomä, A.; Van Beusekom, J.E.E.; Holtappels, M.; Winter, C. Abrupt Emergence of a Large Pockmark Field in the German Bight, Southeastern North Sea. *Sci. Rep.* **2017**, *7*, 5150. [CrossRef] [PubMed]
6. Vaular, E.N.; Barth, T.; Haflidason, H. The Geochemical Characteristics of the Hydrate-Bound Gases from the Nyegga Pockmark Field, Norwegian Sea. *Org. Geochem.* **2010**, *41*, 437–444. [CrossRef]
7. Solheim, A.; Elverhøi, A. A Pockmark Field in the Central Barents Sea; Gas from a Petrogenic Source? *Polar Res.* **1985**, *3*, 11–19. [CrossRef]
8. Gay, A.; Lopez, M.; Ondreas, H.; Charlou, J.L.; Sermondadaz, G.; Cochonat, P. Seafloor Facies Related to Upward Methane Flux within a Giant Pockmark of the Lower Congo Basin. *Mar. Geol.* **2006**, *226*, 81–95. [CrossRef]
9. Roy, S.; Senger, K.; Hovland, M.; Römer, M.; Braathen, A. Geological Controls on Shallow Gas Distribution and Seafloor Seepage in an Arctic Fjord of Spitsbergen, Norway. *Mar. Pet. Geol.* **2019**, *107*, 237–254. [CrossRef]
10. Micallef, A.; Averes, T.; Hoffmann, J.; Crutchley, G.; Mountjoy, J.J.; Person, M.; Cohen, D.; Woelz, S.; Bury, S.J.; Ahaneku, C.V.; et al. Multiple Drivers and Controls of Pockmark Formation across the Canterbury Margin, New Zealand. *Basin Res.* **2022**, *34*, 1374–1399. [CrossRef]
11. Coughlan, M.; Roy, S.; O'Sullivan, C.; Clements, A.; O'Toole, R.; Plets, R. Geological Settings and Controls of Fluid Migration and Associated Seafloor Seepage Features in the North Irish Sea. *Mar. Pet. Geol.* **2021**, *123*, 104762. [CrossRef]
12. Panieri, G.; Bünz, S.; Fornari, D.J.; Escartin, J.; Serov, P.; Jansson, P.; Torres, M.E.; Johnson, J.E.; Hong, W.L.; Sauer, S.; et al. An Integrated View of the Methane System in the Pockmarks at Vestnesa Ridge, 79° N. *Mar. Geol.* **2017**, *390*, 282–300. [CrossRef]
13. de Prunelé, A.; Ruffine, L.; Riboulot, V.; Peters, C.A.; Croguennec, C.; Guyader, V.; Pape, T.; Bollinger, C.; Bayon, G.; Caprais, J.C.; et al. Focused Hydrocarbon-Migration in Shallow Sediments of a Pockmark Cluster in the Niger Delta (Off Nigeria). *Geochem. Geophys. Geosyst.* **2017**, *18*, 93–112. [CrossRef]
14. King, L.H.; MacLean, B. Pockmarks on the Scotian Shelf. *Bull. Geol. Soc. Am.* **1970**, *81*, 3141–3148. [CrossRef]
15. Roelofse, C.; Alves, T.M.; Gafeira, J. Structural Controls on Shallow Fluid Flow and Associated Pockmark Fields in the East Breaks Area, Northern Gulf of Mexico. *Mar. Pet. Geol.* **2020**, *112*, 104074. [CrossRef]
16. Papatheodorou, G.; Hasiotis, T.; Ferentinos, G. Gas-Charged Sediments in the Aegean and Ionian Seas, Greece. *Mar. Geol.* **1993**, *112*, 171–184. [CrossRef]
17. Serié, C.; Huuse, M.; Schødt, N.H.; Brooks, J.M.; Williams, A. Subsurface Fluid Flow in the Deep-Water Kwanza Basin, Offshore Angola. *Basin Res.* **2017**, *29*, 149–179. [CrossRef]
18. Toker, M.; Tur, H. Shallow Seismic Characteristics and Distribution of Gas in Lacustrine Sediments at Lake Erçek, Eastern Anatolia, Turkey, from High-Resolution Seismic Data. *Environ. Earth Sci.* **2021**, *80*, 727. [CrossRef]

19. Cojean, A.N.Y.; Kremer, K.; Bartosiewicz, M.; Fabbri, S.C.; Lehmann, M.F.; Wirth, S.B. Morphology, Formation, and Activity of Three Different Pockmark Systems in Peri-Alpine Lake Thun, Switzerland. *Front. Water* **2021**, *3*, 666641. [CrossRef]
20. Wenau, S.; Spieß, V.; Pape, T.; Fekete, N. Controlling Mechanisms of Giant Deep Water Pockmarks in the Lower Congo Basin. *Mar. Pet. Geol.* **2017**, *83*, 140–157. [CrossRef]
21. Lawal, M.A.; Bialik, O.M.; Lazar, M.; Waldmann, N.D.; Foubert, A.; Makovsky, Y. Modes of Gas Migration and Seepage on the Salt-Rooted Palmahim Disturbance, Southeastern Mediterranean. *Mar. Pet. Geol.* **2023**, *153*, 106256. [CrossRef]
22. Hovland, M. Elongated Depressions Associated with Pockmarks in the Western Slope of the Norwegian Trench. *Mar. Geol.* **1983**, *51*, 35–46. [CrossRef]
23. Acosta, J.; Munoz, A.; Herranz, P.; Palomo, C.; Ballesteros, M.; Vaquero, M.; Uchupi, E. Pockmarks in the Ibiza Channel and Western End of the Balearic Promontory (Western Mediterranean) Revealed by Multibeam Mapping. *Geo-Mar. Lett.* **2001**, *21*, 123–130. [CrossRef]
24. Barrie, J.V.; Hill, P.R. Holocene Faulting on a Tectonic Margin: Georgia Basin, British Columbia, Canada. *Geo-Mar. Lett.* **2004**, *24*, 86–96. [CrossRef]
25. Riedel, M.; Hähnel, L.; Bialas, J.; Bachmann, A.K.; Gaide, S.; Wintersteller, P.; Klaucke, I.; Bohrmann, G. Controls on Gas Emission Distribution on the Continental Slope of the Western Black Sea. *Front. Earth Sci.* **2021**, *8*, 601254. [CrossRef]
26. Jia, X.; Chen, J.; Tong, S.; Azevedo, L.; Duan, M.; Xu, H.; Chen, S.; Yang, R.; Han, T. Research on the Characteristics of Fluid Escape near the Seabed in Bohai Bay. *Geophys. Prospect.* **2023**. [CrossRef]
27. Tasianas, A.; Bünz, S.; Bellwald, B.; Hammer, Ø.; Planke, S.; Lebedeva-Ivanova, N.; Krassakis, P. High-Resolution 3D Seismic Study of Pockmarks and Shallow Fluid Flow Systems at the Snøhvit Hydrocarbon Field in the SW Barents Sea. *Mar. Geol.* **2018**, *403*, 247–261. [CrossRef]
28. Andrews, B.D.; Brothers, L.L.; Barnhardt, W.A. Automated Feature Extraction and Spatial Organization of Seafloor Pockmarks, Belfast Bay, Maine, USA. *Geomorphology* **2010**, *124*, 55–64. [CrossRef]
29. Brothers, L.L.; Kelley, J.T.; Belknap, D.F.; Barnhardt, W.A.; Andrews, B.D.; Legere, C.; Hughes Clarke, J.E. Shallow Stratigraphic Control on Pockmark Distribution in North Temperate Estuaries. *Mar. Geol.* **2012**, *329–331*, 34–45. [CrossRef]
30. Judd, A.G.; Hovland, M. *Seabed Fluid Flow: The Impact of Geology, Biology and the Marine Environment*; Cambridge University Press: Cambridge, UK, 2007; ISBN 9780521819503.
31. Broster, B.E.; Legere, C.L. Seafloor Pockmarks and Gas Seepages, Northwestern Bay of Fundy, New Brunswick, Canada. *Atl. Geol.* **2018**, *54*, 1–20. [CrossRef]
32. Field, M.E.; Jennings, A.E. Seafloor Gas Seeps Triggered by a Northern California Earthquake. *Mar. Geol.* **1987**, *77*, 39–51. [CrossRef]
33. Kuşçu, I.; Okamura, M.; Matsuoka, H.; Gökaşan, E.; Awata, Y.; Tur, H.; Şimşek, M.; Keçer, M. Seafloor Gas Seeps and Sediment Failures Triggered by the August 17, 1999 Earthquake in the Eastern Part of the Gulf of İzmit, Sea of Marmara, NW Turkey. *Mar. Geol.* **2005**, *215*, 193–214. [CrossRef]
34. Géli, L.; Henry, P.; Zitter, T.; Dupré, S.; Tryon, M.; Çağatay, M.N.; de Lépinay, B.M.; Le Pichon, X.; Şengör, A.M.C.; Görür, N.; et al. Gas Emissions and Active Tectonics within the Submerged Section of the North Anatolian Fault Zone in the Sea of Marmara. *Earth Planet Sci. Lett.* **2008**, *274*, 34–39. [CrossRef]
35. Sarıtaş, H.; Çifçi, G.; Géli, L.; Thomas, Y.; Marsset, B.; Henry, P.; Grall, C.; Rochat, A. Gas Occurrence and Shallow Conduit Systems in the Western Sea of Marmara: A Review and New Acoustic Evidence. *Geo-Mar. Lett.* **2018**, *38*, 385–402. [CrossRef]
36. Fischer, D.; Mogollón, J.M.; Strasser, M.; Pape, T.; Bohrmann, G.; Fekete, N.; Spiess, V.; Kasten, S. Subduction Zone Earthquake as Potential Trigger of Submarine Hydrocarbon Seepage. *Nat. Geosci.* **2013**, *6*, 647–651. [CrossRef]
37. Römer, M.; Riedel, M.; Scherwath, M.; Heesemann, M.; Spence, G.D. Tidally Controlled Gas Bubble Emissions: A Comprehensive Study Using Long-Term Monitoring Data from the NEPTUNE Cabled Observatory Offshore Vancouver Island. *Geochem. Geophys. Geosyst.* **2016**, *17*, 3797–3814. [CrossRef]
38. Lapham, L.; Wilson, R.; Riedel, M.; Paull, C.K.; Holmes, M.E. Temporal Variability of in Situ Methane Concentrations in Gas Hydrate-Bearing Sediments near Bullseye Vent, Northern Cascadia Margin. *Geochem. Geophys. Geosyst.* **2013**, *14*, 2445–2459. [CrossRef]
39. Hasiotis, T.; Papatheodorou, G.; Kastanos, N.; Ferentinos, G. A Pockmark Field in the Patras Gulf (Greece) and Its Activation during the 14/7/93 Seismic Event. *Mar. Geol.* **1996**, *130*, 333–344. [CrossRef]
40. Christodoulou, D.; Papatheodorou, G.; Fakiris, E.; Etiope, G.; Ferentinos, G. The Activation of the Patras Gulf, Western Greece, Pockmark Field Triggered by the Mw=6.4R June 8, 2008 Earthquake. In Proceedings of the 10th International Conference on Gas Geochemistry, Cluj-Napoca, Romania, 14–21 September 2009; p. 30.
41. Christodoulou, D. Geophysical, Sedimentological Study—Remote Sensing on Pockmarks in Active Seismogenic Areas. Ph.D. Thesis, University of Patras, Patras, Greece, 2010.
42. Papatheodorou, G.; Christodoulou, D.; Geraga, M.; Etiope, G.; Ferentinos, G. The Pockmark Field of the Gulf of Patras: An Ideal Natural Laboratory for Studying Seabed Fluid Flow. In *Field Trips Guide Book "Sedimentology of Western and Central Greece from Triassic to Recent, Proceedings of the 25th IAS Meeting of Sedimentology, Patras, Greece, 4–7 September 2007*; University of Patras: Patras, Greece, 2007; pp. 43–62.
43. Ravasopoulos, J.; Papatheodorou, G.; Kapolos, J.; Geraga, M.; Koliadima, A.; Xenos, K. A Promising Methodology for the Detection of Pockmarks Activation in Nearshore Sediments. *Instrum. Sci. Technol.* **2002**, *30*, 139–155. [CrossRef]

44. Hellenic Survey of Geology and Mineral Exploration Geological Map of Greece 1:500,000. Available online: https://gaia.igme.gr/portal/apps/webappviewer/index.html?id=61dc7b67790944a198d4dbdc876d1a3c (accessed on 5 August 2023).
45. Kokkalas, S.; Xypolias, P.; Koukouvelas, I.; Doutsos, T. *Postcollisional Contractional and Extensional Deformation in the Aegean Region*; Geological Society of America: Patras, Greece, 2006; Volume 409.
46. Institute of Geodynamics of the National Observatory of Athens. Available online: https://Bbnet.Gein.Noa.Gr/HL/Databases/Database (accessed on 5 August 2023).
47. Doutsos, T.; Poulimenos, G. Geometry and Kinematics of Active Faults and Their Seismotectonic Significance in the Western Corinth-Patras Rift (Greece). *J. Struct. Geol.* **1992**, *14*, 689–699. [CrossRef]
48. Flotté, N.; Sorel, D.; Müller, C.; Tensi, J. Along Strike Changes in the Structural Evolution over a Brittle Detachment Fault: Example of the Pleistocene Corinth-Patras Rift (Greece). *Tectonophysics* **2005**, *403*, 77–94. [CrossRef]
49. Melis, N.S.; Brooks, M.; Pearce, R.G. A Microearthquake Study in the Gulf of Patras Region, Western Greece, and Its Seismotectonic Interpretation. *Geophys. J. Int.* **1989**, *98*, 515–524. [CrossRef]
50. Ferentinos, G.; Brooks, M.; Doutsos, T. Quaternary Tectonics in the Gulf of Patras, Western Greece. *J. Struct. Geol.* **1985**, *7*, 713–717. [CrossRef]
51. Chronis, G.; Piper, D.J.W.; Anagnostou, C. Late Quaternary Evolution of the Gulf of Patras, Greece: Tectonism, Deltaic Sedimentation and Sea-Level Change. *Mar. Geol.* **1991**, *97*, 191–209. [CrossRef]
52. Haddad, A.; Ganas, A.; Kassaras, I.; Lupi, M. Seismicity and Geodynamics of Western Peloponnese and Central Ionian Islands: Insights from a Local Seismic Deployment. *Tectonophysics* **2020**, *778*, 228353. [CrossRef]
53. Plicka, V.; Sokos, E.; Tselentis, G.-A.; Zahradník, J. The Patras Earthquake (14 July 1993): Relative Roles of Source, Path and Site Effects. *J. Seismol.* **1998**, *2*, 337–349. [CrossRef]
54. Tselentis, G.-A. Fault Lengths During the Patras 1993 Earthquake Sequence as Estimated from the Pulse Width of Initial P Wave. *Pure Appl. Geophys.* **1998**, *152*, 75–89. [CrossRef]
55. Marinaro, G.; Etiope, G.; Bue, N.L.; Favali, P.; Papatheodorou, G.; Christodoulou, D.; Furlan, F.; Gasparoni, F.; Ferentinos, G.; Masson, M.; et al. Monitoring of a Methane-Seeping Pockmark by Cabled Benthic Observatory (Patras Gulf, Greece). *Geo-Mar. Lett.* **2006**, *26*, 297–302. [CrossRef]
56. Koukouvelas, I.K.; Kokkalas, S.; Xypolias, P. Surface Deformation during the Mw 6.4 (8 June 2008) Movri Mountain Earthquake in the Peloponnese, and Its Implications for the Seismotectonics of Western Greece. *Int. Geol. Rev.* **2010**, *52*, 249–268. [CrossRef]
57. Christodoulou, D.; Papatheodorou, G.; Ferentinos, G.; Masson, M. Active Seepage in Two Contrasting Pockmark Fields in the Patras and Corinth Gulfs, Greece. *Geo-Mar. Lett.* **2003**, *23*, 194–199. [CrossRef]
58. Milionis, N.; Kokoromitis, A. *Technical Report of Evaluation of Geotechnical Survey Results (B2 Phase of Geotechnical Surveys)*; New Port of Patras: Patras, Greece, 2007.
59. Booth, J.S.; Sangrey, D.A.; Fugate, J.K. A Nomogram for Interpreting Slope Stability of Fine-Grained Deposits in Modern and Ancient-Marine Environments. *J. Sediment. Petrol.* **1985**, *55*, 29–36. [CrossRef]
60. Allen, J.R.L. *Principles of Physical Sedimentology*; Chapman & Hall: London, UK, 1985.
61. Damuth, J.E. Echo Character of the Western Equatorial Atlantic Floor and Its Relationship to the Dispersal and Distribution of Terrigenous Sediments. *Mar. Geol.* **1975**, *18*, 17–45. [CrossRef]
62. Kordella, S.; Christodoulou, D.; Fakiris, E.; Geraga, M.; Kokkalas, S.; Marinaro, G.; Iatrou, M.; Ferentinos, G.; Papatheodorou, G. Gas Seepage-Induced Features in the Hypoxic/Anoxic, Shallow, Marine Environment of Amfilochia Bay, Amvrakikos Gulf (Western Greece). *Geosciences* **2021**, *11*, 27. [CrossRef]
63. Garcia-Gil, S.; Vilas, F.; Garcia-Garcia, A. Shallow Gas Features in Incised-Valley Fills (Ría de Vigo, NW Spain): A Case Study. *Cont. Shelf Res.* **2002**, *22*, 2303–2315. [CrossRef]
64. Luo, D.; Cai, F.; Li, Q.; Yan, G.; Sun, Y.; Li, A.; Dong, G. Geophysical Evidence for Submarine Methane Seepage on the Western Slope of Okinawa Trough. *Front. Earth Sci.* **2022**, *10*, 985597. [CrossRef]
65. Roy, S.; Hovland, M.; Braathen, A. Evidence of Fluid Seepage in Grønfjorden, Spitsbergen: Implications from an Integrated Acoustic Study of Seafloor Morphology, Marine Sediments and Tectonics. *Mar. Geol.* **2016**, *380*, 67–78. [CrossRef]
66. Papatheodorou, G.; Geraga, M.; Christodoulou, D.; Fakiris, E.; Iatrou, M.; Georgiou, N.; Dimas, X.; Ferentinos, G. The Battle of Lepanto Search and Survey Mission (1971–1972) by Throckmorton, Edgerton and Yalouris: Following Their Traces Half a Century Later Using Marine Geophysics. *Remote Sens.* **2021**, *13*, 3292. [CrossRef]
67. Koch, S.; Berndt, C.; Bialas, J.; Haeckel, M.; Crutchley, G.; Papenberg, C.; Klaeschen, D.; Greinert, J. Gas-Controlled Seafloor Doming. *Geology* **2015**, *43*, 571–574. [CrossRef]
68. Greinert, J.; Artemov, Y.; Egorov, V.; De Batist, M.; McGinnis, D. 1300-m-High Rising Bubbles from Mud Volcanoes at 2080 m in the Black Sea: Hydroacoustic Characteristics and Temporal Variability. *Earth Planet Sci. Lett.* **2006**, *244*, 1–15. [CrossRef]
69. Klaucke, I.; Sahling, H.; Weinrebe, W.; Blinova, V.; Bürk, D.; Lursmanashvili, N.; Bohrmann, G. Acoustic Investigation of Cold Seeps Offshore Georgia, Eastern Black Sea. *Mar. Geol.* **2006**, *231*, 51–67. [CrossRef]
70. Etiope, G.; Christodoulou, D.; Kordella, S.; Marinaro, G.; Papatheodorou, G. Offshore and Onshore Seepage of Thermogenic Gas at Katakolo Bay (Western Greece). *Chem. Geol.* **2013**, *339*, 115–126. [CrossRef]
71. De Beukelaer, S.M.; MacDonald, I.R.; Guinnasso, N.L.; Murray, J.A. Distinct Side-Scan Sonar, RADARSAT SAR, and Acoustic Profiler Signatures of Gas and Oil Seeps on the Gulf of Mexico Slope. *Geo-Mar. Lett.* **2003**, *23*, 177–186. [CrossRef]

72. Obzhirov, A.; Shakirov, R.; Salyuk, A.; Suess, E.; Biebow, N.; Salomatin, A. Relations between Methane Venting, Geological Structure and Seismo-Tectonics in the Okhotsk Sea. *Geo-Mar. Lett.* **2004**, *24*, 135–139. [CrossRef]
73. Kim, Y.J.; Cheong, S.; Chun, J.H.; Cukur, D.; Kim, S.P.; Kim, J.K.; Kim, B.Y. Identification of Shallow Gas by Seismic Data and AVO Processing: Example from the Southwestern Continental Shelf of the Ulleung Basin, East Sea, Korea. *Mar. Pet. Geol.* **2020**, *117*, 104346. [CrossRef]
74. Guinasso, N.L.; Schink, D.R. A Simple Physiochemical Acoustic Model of Methane Bubbles Rising in the Sea. In *Study of Naturally Occurring Hydrocarbons in the Gulf of Mexico*; Texas A&M University, College of Geosciences: College Station, TX, USA, 1973.
75. Rodes, N.; Betlem, P.; Senger, K.; Römer, M.; Hodson, A.; Liira, M.; Birchall, T.; Roy, S.; Noormets, R.; Smyrak-Sikora, A.; et al. Active Gas Seepage in Western Spitsbergen Fjords, Svalbard Archipelago: Spatial Extent and Geological Controls. *Front. Earth Sci.* **2023**, *11*, 1173477. [CrossRef]
76. Parcharidis, I.; Kokkalas, S.; Fountoulis, I.; Foumelis, M. Detection and Monitoring of Active Faults in Urban Environments: Time Series Interferometry on the Cities of Patras and Pyrgos (Peloponnese, Greece). *Remote Sens.* **2009**, *1*, 676–696. [CrossRef]
77. Koukis, G.; Sabatakakis, N.; Tsiambaos, G.; Katrivesis, N. Engineering Geological Approach to the Evaluation of Seismic Risk in Metropolitan Regions: Case Study of Patras, Greece. *Bull. Eng. Geol. Environ.* **2005**, *64*, 219–235. [CrossRef]
78. Katrivesis, N. *Engineering Geological Conditions in the Broader Area of Patras*; University of Patras: Patras, Greece, 2005.
79. Morley, C.K.; Nelson, R.A.; Patton, T.L.; Munn, S.G. Transfer Zones in the East African Rift System and Their Relevance to Hydrocarbon Exploration in Rifts1. *Am. Assoc. Pet. Geol. Bull.* **1990**, *74*, 1234–1253. [CrossRef]
80. Milkov, A.V.; Etiope, G. Revised Genetic Diagrams for Natural Gases Based on a Global Dataset of >20,000 Samples. *Org. Geochem.* **2018**, *125*, 109–120. [CrossRef]
81. Pilcher, R.; Argent, J. Mega-Pockmarks and Linear Pockmark Trains on the West African Continental Margin. *Mar. Geol.* **2007**, *244*, 15–32. [CrossRef]
82. Moss, J.L.; Cartwright, J.; Moore, R. Evidence for Fluid Migration Following Pockmark Formation: Examples from the Nile Deep Sea Fan. *Mar. Geol.* **2012**, *303–306*, 1–13. [CrossRef]
83. Audsley, A.; Bradwell, T.; Howe, J.A.; Baxter, J.M. Distribution and Classification of Pockmarks on the Seabed around Western Scotland. *J. Maps* **2019**, *15*, 807–817. [CrossRef]
84. Hovland, M.; Gardner, J.V.; Judd, A.G. The Significance of Pockmarks to Understanding Fluid Flow Processes and Geohazards. *Geofluids* **2002**, *2*, 127–136. [CrossRef]
85. Gafeira, J.; Long, D.; Diaz-Doce, D. Semi-Automated Characterisation of Seabed Pockmarks in the Central North Sea. *Near Surf. Geophys.* **2012**, *10*, 301–312. [CrossRef]
86. Picard, K.; Radke, L.C.; Williams, D.K.; Nicholas, W.A.; Justy Siwabessy, P.; Howard, F.J.F.; Gafeira, J.; Przeslawski, R.; Huang, Z.; Nichol, S. Origin of High Density Seabed Pockmark Fields and Their Use in Inferring Bottom Currents. *Geosciences* **2018**, *8*, 195. [CrossRef]
87. Hovland, M.; Vasshus, S.; Heggland, R. Pockmarks in the Norwegian Trench—Some New Observations. In Proceedings of the 4th Conference on Gas in Marine Sediments, Varna, Bulgaria, 28–30 September 1996.
88. Hasiotis, T.; Papatheodorou, G.; Ferentinos, G. A String of Large and Deep Gas-Induced Depressions (Pockmarks) Offshore Killini Peninsula, Western Greece. *Geo-Mar. Lett.* **2002**, *22*, 142–149. [CrossRef]
89. Gay, A.; Lopez, M.; Berndt, C.; Séranne, M. Geological Controls on Focused Fluid Flow Associated with Seafloor Seeps in the Lower Congo Basin. *Mar. Geol.* **2007**, *244*, 68–92. [CrossRef]
90. Söderberg, P.; Flodén, T. Gas Seepages, Gas Eruptions and Degassing Structures in the Seafloor along the Strömma Tectonic Lineament in the Crystalline Stockholm Archipelago, East Sweden. *Cont. Shelf Res.* **1992**, *12*, 1157–1171. [CrossRef]
91. Webb, K.E.; Hammer, Ø.; Lepland, A.; Gray, J.S. Pockmarks in the Inner Oslofjord, Norway. *Geo-Mar. Lett.* **2009**, *29*, 111–124. [CrossRef]
92. Schattner, U.; Lazar, M.; Souza, L.A.P.; ten Brink, U.; Mahiques, M.M. Pockmark Asymmetry and Seafloor Currents in the Santos Basin Offshore Brazil. *Geo-Mar. Lett.* **2016**, *36*, 457–464. [CrossRef]
93. Papatheodorou, G.; Kontopoulos, N. Determination of Sediment Transport Directions Using the "McLaren" Method. Examples from the Patras and Amvrakikos Gulfs, Greece. *Bull. Geol. Soc. Greece* **1998**, *32*, 145–155.
94. Rogers, J.N.; Kelley, J.T.; Belknap, D.F.; Gontz, A.; Barnhardt, W.A. Shallow-Water Pockmark Formation in Temperate Estuaries: A Consideration of Origins in the Western Gulf of Maine with Special Focus on Belfast Bay. *Mar. Geol.* **2006**, *225*, 45–62. [CrossRef]
95. Kelley, J.T.; Dickson, S.M.; Belknap, D.F.; Barnhardt, W.A.; Henderson, M. Giant Sea-Bed Pockmarks: Evidence for Gas Escape from Belfast Bay, Maine. *Geology* **1994**, *22*, 59–62. [CrossRef]
96. Dupré, S.; Woodside, J.; Klaucke, I.; Mascle, J.; Foucher, J.P. Widespread Active Seepage Activity on the Nile Deep Sea Fan (Offshore Egypt) Revealed by High-Definition Geophysical Imagery. *Mar. Geol.* **2010**, *275*, 1–19. [CrossRef]
97. Olu-Le Roy, K.; Sibuet, M.; Fiala-Médioni, A.; Gofas, S.; Salas, C.; Mariotti, A.; Foucher, J.-P.; Woodside, J. Cold Seep Communities in the Deep Eastern Mediterranean Sea: Composition, Symbiosis and Spatial Distribution on Mud Volcanoes. *Deep. Sea Res. Part I Oceanogr. Res. Pap.* **2004**, *51*, 1915–1936. [CrossRef]
98. Sibuet, M.; Olu, K. Biogeography, Biodiversity and Fluid Dependence of Deep-Sea Cold-Seep Communities at Active and Passive Margins. *Deep Sea Res. 2 Top Stud. Oceanogr.* **1998**, *45*, 517–567. [CrossRef]

99. Klaucke, I.; Masson, D.G.; Jörg Petersen, C.; Weinrebe, W.; Ranero, C.R. Multifrequency Geoacoustic Imaging of Fluid Escape Structures Offshore Costa Rica: Implications for the Quantification of Seep Processes. *Geochem. Geophys. Geosyst.* **2008**, *9*, Q04010. [CrossRef]
100. Zitter, T.A.C.; Huguen, C.; Woodside, J.M. Geology of Mud Volcanoes in the Eastern Mediterranean from Combined Sidescan Sonar and Submersible Surveys. *Deep Sea Res. 1 Oceanogr. Res. Pap.* **2005**, *52*, 457–475. [CrossRef]
101. Dando, P.R.; Austen, M.C.; Burke, R.A.; Kendall, M.A.; Kennicutt, M.C.; Judd, A.G.; Moore, D.C.; O'Hara, S.C.M.; Schmalijohann, R.; Southward, A.J. Ecology of a North Sea Pockmark with an Active Methane Seep. *Mar. Ecol. Prog. Ser.* **1991**, *70*, 49–63. [CrossRef]
102. Webb, K.E.; Barnes, D.K.A.; Planke, S. Pockmarks: Refuges for Marine Benthic Biodiversity. *Limnol. Oceanogr.* **2009**, *54*, 1776–1788. [CrossRef]
103. Baltzer, A.; Ehrhold, A.; Rigolet, C.; Souron, A.; Cordier, C.; Clouet, H.; Dubois, S.F. Geophysical Exploration of an Active Pockmark Field in the Bay of Concarneau, Southern Brittany, and Implications for Resident Suspension Feeders. *Geo-Mar. Lett.* **2014**, *34*, 215–230. [CrossRef]
104. Webb, K.E.; Barnes, D.K.A.; Gray, J.S. Benthic Ecology of Pockmarks in the Inner Oslofjord, Norway. *Mar. Ecol. Prog. Ser.* **2009**, *387*, 15–25. [CrossRef]
105. Zhang, K.; Guan, Y.; Song, H.; Fan, W.; Li, H.; Kuang, Y.; Geng, M. A Preliminary Study on Morphology and Genesis of Giant and Mega Pockmarks near Andu Seamount, Nansha Region (South China Sea). *Mar. Geophys. Res.* **2020**, *41*, 2. [CrossRef]
106. Froelich, P.N.; Klinkhammer, G.P.; Bender, M.L.; Luedtke, N.A.; Heath, G.R.; Cullen, D.; Dauphin, P.; Hammond, D.; Hartman, B.; Maynard, V. Early Oxidation of Organic Matter in Pelagic Sediments of the Eastern Equatorial Atlantic: Suboxic Diagenesis. *Geochim. Cosmochim. Acta* **1979**, *43*, 1075–1090. [CrossRef]
107. Capone, D.G.; Kiene, R.P. Comparison of Microbial Dynamics in Marine and Freshwater Sediments: Contrasts in Anaerobic Carbon Catabolism. *Limnol. Oceanogr.* **1988**, *33*, 725–749. [CrossRef]
108. García-García, A.; Orange, D.L.; Miserocchi, S.; Correggiari, A.; Langone, L.; Lorenson, T.D.; Trincardi, F.; Nittrouer, C.A. What Controls the Distribution of Shallow Gas in the Western Adriatic Sea? *Cont. Shelf Res.* **2007**, *27*, 359–374. [CrossRef]
109. Weschenfelder, J.; Klein, A.H.F.; Green, A.N.; Aliotta, S.; de Mahiques, M.M.; Ayres Neto, A.; Terra, L.C.; Corrêa, I.C.S.; Calliari, L.J.; Montoya, I.; et al. The Control of Palaeo-Topography in the Preservation of Shallow Gas Accumulation: Examples from Brazil, Argentina and South Africa. *Estuar. Coast Shelf Sci.* **2016**, *172*, 93–107. [CrossRef]
110. Piper, D.J.W.; Stamatopoulos, L.; Poulimenos, G.; Doutsos, T.; Kontopoulos, N. Quaternary History of the Gulfs of Patras and Corinth, Greece. *Z. Für Geomorphol.* **1991**, *34*, 451–458. [CrossRef]
111. Leifer, I.; MacDonald, I. Dynamics of the Gas Flux from Shallow Gas Hydrate Deposits: Interaction between Oily Hydrate Bubbles and the Oceanic Environment. *Earth Planet Sci. Lett.* **2003**, *210*, 411–424. [CrossRef]
112. Greinert, J.; Lewis, K.B.; Bialas, J.; Pecher, I.A.; Rowden, A.; Bowden, D.A.; De Batist, M.; Linke, P. Methane Seepage along the Hikurangi Margin, New Zealand: Overview of Studies in 2006 and 2007 and New Evidence from Visual, Bathymetric and Hydroacoustic Investigations. *Mar. Geol.* **2010**, *272*, 6–25. [CrossRef]
113. Kiratzi, A.; Louvari, E. Focal Mechanisms of Shallow Earthquakes in the Aegean Sea and the Surrounding Lands Determined by Waveform Modelling: A New Database. *J. Geodyn.* **2003**, *36*, 251–274. [CrossRef]
114. Serpetsidaki, A.; Elias, P.; Ilieva, M.; Bernard, P.; Briole, P.; Deschamps, A.; Lambotte, S.; Lyon-Caen, H.; Sokos, E.; Tselentis, G.A. New Constraints from Seismology and Geodesy on the Mw = 6.4 2008 Movri (Greece) Earthquake: Evidence for a Growing Strike-Slip Fault System. *Geophys. J. Int.* **2014**, *198*, 1373–1386. [CrossRef]
115. Tselentis, G.; Melis, N.; Sokos, E. Earthquake Sequence as It Was Recorded by the Patras Seismic Network. In Proceedings of the 7th Congress of the Geological Society of Greece, Thessaloniki, Greece, 25–27 May 1994; Bulletin of the Geological Society of Greece. pp. 159–165.